ANL-8036

ANL-8036

EXPERIMENTAL EVALUATION OF FISSION-GAS RELEASE IN LMFBR SUBASSEMBLIES USING AN ELECTRICALLY HEATED TEST SECTION WITH SODIUM AS COOLANT

R. E. Wilson, J. B. van Erp, T. C. Chawla,
E. L. Kimont, and R. D. Baldwin

BASE TECHNOLOGY

U of C-AUA-USAEC

ARGONNE NATIONAL LABORATORY, ARGONNE, ILLINOIS

Prepared for the U.S. ATOMIC ENERGY COMMISSION
Division of Reactor Research and Development
under Contract W-31-109-Eng-38

DISCLAIMER

Printed in the United States of America

Available from National Technical Information Service
5285 Port Royal Road
Springfield, Virginia 22151
Price: Printed Copy $5.45; Microfiche $1.45

ANL-8036
LMFBR Safety
(UC-79p)

ARGONNE NATIONAL LABORATORY
9700 South Cass Avenue
Argonne, Illinois 60439

EXPERIMENTAL EVALUATION OF FISSION-GAS RELEASE IN LMFBR SUBASSEMBLIES USING AN ELECTRICALLY HEATED TEST SECTION WITH SODIUM AS COOLANT

by

R. E. Wilson, J. B. van Erp, T. C. Chawla,
E. L. Kimont, and R. D. Baldwin

Reactor Analysis and Safety Division

July 1973

THIS PAGE
WAS INTENTIONALLY
LEFT BLANK

TABLE OF CONTENTS

LIST OF FIGURES

LIST OF FIGURES

LIST OF FIGURES

LIST OF FIGURES

LIST OF FIGURES

LIST OF FIGURES

LIST OF FIGURES

TABLE

NOMENCLATURE

Symbol	Equivalent Computer Symbol	Description
h	H	Heat-transfer coefficient between external cladding surface temperature and coolant bulk temperature
$\dot{m}$	MF	Coolant mass flow rate
P_e	PE	Coolant pressure at test-section exit
P_g	PG	Gas-plenum pressure
P_i	PI	Coolant pressure at test-section inlet
P_s	PS	System coolant pressure at gas-release point
q"	Q"	Heat flux
T_e	TE	Coolant temperature at test-section exit
T_g	TG	Gas-plenum temperature
T_i	TI	Coolant temperature at test-section inlet
ΔT	DT	Cladding-temperature rise in affected pin-surface area
Z	Z	Relative axial position of gas-release needle with respect to internal thermocouple of heater pin to be impinged upon
Ar	AR	Argon
Xe	XE	Xenon
	NID	Needle internal diameter

Superscripts

* denotes value of quantity during gas release.

EXPERIMENTAL EVALUATION OF FISSION-GAS RELEASE IN LMFBR SUBASSEMBLIES USING AN ELECTRICALLY HEATED TEST SECTION WITH SODIUM AS COOLANT

by

R. E. Wilson, J. B. van Erp, T. C. Chawla,
E. L. Kimont, and R. D. Baldwin

ABSTRACT

A description is given of an out-of-pile experiment which simulated fission-gas release in current-design uranium-oxide fuel subassemblies of liquid-metal-cooled fast breeder reactors (LMFBR's) and which was performed to evaluate the potential for pin-to-pin failure propagation due to thermal transients induced in adjacent fuel pins. A sodium-cooled test section containing three electrically heated pins was used. Gas (argon or xenon), injected as a jet through a needle protruding into the flow cross-sectional area of the test section, was made to impinge on one of the heater pins. Data are presented regarding the measured cladding-temperature rise and the calculated local heat-transfer coefficient in the impingement area, with the following parameters: gas type, needle internal diameter, heat flux, coolant flow rate, gas-plenum pressure and temperature, and axial location with respect to the gas jet. The cladding-temperature rises measured represent upper values, since the conditions under which they were obtained are conservative. There are two reasons for this: (a) The gas-release rates correspond to those that would prevail if the internal resistance to the flow of gas, between the gas plenum and the point of release of the fuel pin, were negligibly small; (b) the tests were performed under steady-state conditions, whereas, under actual reactor conditions, the gas-release rates would be decreasing with time because of the fixed fission-gas inventory.

For a narrow range of gas-release rates under subsonic and near-subsonic conditions, cladding-temperature rises were found to occur in the impingement area, for the above conservative conditions, of up to ~240°C at a heat flux of 250 W/cm^2.

I. INTRODUCTION

Experiments performed at Argonne National Laboratory to evaluate the potential of fission-gas release in LMFBR fuel subassemblies to lead to pin-to-pin failure propagation due to induced thermal transients in adjacent fuel pins have been reported on regularly.[1-14] This report deals mainly with tests performed from March 1972 to January 1973 and gives primarily the experimental data.

Fission-gas-release experiments with sodium as coolant performed before December 1971[8,9,14] dealt primarily with release under operating conditions far into the sonic range. The present experiments are focused on the subsonic and near-subsonic range.

The authors recognize that the upper values of the gas-release rates for which test runs were performed may not represent values that are possible in an actual current-design LMFBR fuel pin because of the presence of flow resistances in the gas-release path due to, e.g., the neutron reflector and cracked fuel pellets. In the experiments reported here, these gas-flow resistances were not included in the simulation, so that, for the same size of the gas-release aperture from which the gas is injected into the coolant subchannel, higher gas-release rates were possible for the experiment performed than might occur for fission-gas release from a current-design uranium oxide LMFBR fuel pin. It was believed, however, that, once the test apparatus was set up and performing well, it was preferable to take too many data than too few. The additional data are helpful in the interpretation of the various phenomena involved. Furthermore, the boundary between the gas-release rates that are realistic and those that are not is not well-defined at present, and depends on a large number of parameters (uranium oxide density, pellet-to-cladding gap, burnup, etc.) that may be different for future LMFBR fuels.

II. DESCRIPTION OF EXPERIMENT

The test section used and the test procedures followed have been described earlier.[8,14] The test section and the sodium test loop are described briefly in Appendixes A and B.

In the experiments reported here, fission-gas release in an LMFBR fuel subassembly due to random failure of a single fuel pin was simulated out-of-pile using an electrically heated, three-pin test section with sodium as coolant and with argon or xenon as fission-gas simulant. The gas was released through a needle protruding into the cross-sectional coolant flow area of the test section (see Fig. A.1). Particular attention was given to the gas-release mode in which a gas jet, emanating from a failed fuel pin, impinges on an adjacent fuel pin, thus locally affecting the heat-transfer mechanism.

An attempt was made to cover as wide as possible a range of gas-release rates, both by varying the gas-plenum pressure (from a value close to the local system coolant pressure to the end-of-life value) and by varying the internal diameter of the needle through which the gas was released. The smallest needle used had an internal diameter of 0.033 cm. This aperture represents the approximate value of the lower limit of the range of apertures to be tested, because smaller apertures (a) result in gas jets that are easily deflected by the coolant flow and may not reach the opposite pins and (b) were found to plug easily during the experimental runs, which would probably also be the case for fission-gas release in an actual LMFBR fuel subassembly.

In December 1971, during test runs reported earlier, a loss-of-flow incident, caused by accumulation of gas bubbles in the electromagnetic pump of the sodium loop used for the present experiment, resulted in destruction of the heater pins of the three-pin test section. Subsequently, the test section was restored to its previous condition (using new heaters of the same type as those used before the incident), the sole difference being that some additional spacers were mounted in the inlet region of the test section in order to maintain closer control over the spacing of the heater pins. In addition, the heater pin to be impinged upon was provided with a drive mechanism that allowed adjustment of the axial position of this pin over a maximum range of ~1.0 cm. This latter design feature, aimed at obtaining data regarding the extent and the fine structure of the impingement area, was included in view of the fact that the heater pins (fabricated by Watlow Electric Manufacturing Co.) could be delivered with internal thermocouples at a single axial location only.

The main limitations on the range of operating conditions of the sodium loop for the experiments in question were due to the limited capability of the loop for separating the injected gas from the coolant in the upper plenum. This resulted in some gas being carried under, which led subsequently to accumulation of gas in the pump region. The amount of gas carried under in the upper plenum depends on the coolant mass flow rate and the gas volumetric flow rate.

For any test run, the time period between initiation of gas injection and the moment the first gas bubbles reached the pump amounted to a minimum of ~60 sec for the test series reported on here. For any test run, all data were taken during the first 30 sec following initiation of gas injection, so that a possible coolant-flow reduction due to accumulation of gas bubbles in the pump region had no effect on the data. However, for those cases in which a large amount of gas was carried under in the upper plenum, the arrival of the gas bubbles in the pump region would cause a rapid decrease of the coolant flow, which could in turn result in damage to the heaters and the test section. To avoid any possible damage to the experimental equipment, limits had to be imposed on the injection rate of the gas.

III. PRESENTATION OF EXPERIMENTAL DATA

Table I summarizes the experimental data obtained, including the range of the operating conditions covered in the test runs. Figures 1-21 and 22-42 give, respectively, the cladding-temperature rise ΔT and the heat-transfer coefficient h^* in the impingement area, as a function of both the relative position Z of the gas-release point with respect to the internal thermocouples and the ratio of gas-plenum pressure to system coolant pressure, P_g/P_s. All data were taken for a system coolant pressure, P_s, equal to 4 bar, abs.

TABLE I. Summary of Experimental Data

Fig. No.	Description of Test	Gas Type	Needle ID, cm	q", W/cm²	ṁ, g/sec	T_g, °C	P_g, bar (abs)	Z, cm
1, 22	ΔT and h^* versus Z	Argon	0.058	126	690	510	7	
2, 23	ΔT and h^* versus Z	Argon	0.058	126	690	510	14	
3, 24	ΔT and h^* versus Z	Argon	0.058	126	690	510	21	
4, 25	ΔT and h^* versus Z	Argon	0.058	126	690	510	28	
5, 26	ΔT and h^* versus Z	Argon	0.058	126	690	510	35	
6, 27	ΔT and h^* versus Z	Argon	0.058	126	690	510	41	
7, 28	ΔT and h^* versus Z	Argon	0.058	126	690	510	48	
8, 29	ΔT and h^* versus Z	Argon	0.058	126	690	510	54	
9, 30	ΔT and h^* versus P_g/P_s	Argon	0.058	126	690	510		0
10, 31	ΔT and h^* versus P_g/P_s	Argon	0.058	250	690	510		0
11, 32	ΔT and h^* versus P_g/P_s	Argon	0.058	126	552	510		0
12, 33	ΔT and h^* versus P_g/P_s	Argon	0.058	126	414	510		0
13, 34	ΔT and h^* versus P_g/P_s	Argon	0.058	25	138	510		0
14, 35	ΔT and h^* versus P_g/P_s	Argon	0.058	126	690	720		0
15, 36	ΔT and h^* versus P_g/P_s	Xenon	0.058	126	690	510		0
16, 37	ΔT and h^* versus P_g/P_s	Argon	0.033	126	690	510		0
17, 38	ΔT and h^* versus Z	Argon	0.084	126	690	510		
18, 39	ΔT and h^* versus Z	Argon	0.084	126	690	510		
19, 40	ΔT and h^* versus Z	Argon	0.084	126	690	510		
20, 41	ΔT and h^* versus Z	Argon	0.084	126	690	510		
21, 42	ΔT and h^* versus P_g/P_s	Argon	0.084	126	690	510		0

Appendix D lists all the test runs performed, including the measured operating conditions for each data point. The operating conditions given in the captions of Figs. 1-42 are the nominal values. The test parameters that were varied for the different runs are (1) gas type, (2) needle internal diameter, (3) heat flux q", (4) coolant mass flow rate $\dot{m}$, (5) gas-plenum temperature T_g, and (6) gas-plenum pressure P_g.

All measurements were performed at steady-state conditions for heater-pin power, coolant flow, and gas-plenum pressure and temperature. Furthermore, all test runs were carried out with a coolant temperature of 315°C at the test-section inlet.

The present test runs covered a range of P_g/P_s from ~1.2 to 14.

Nearly all test runs were performed with argon as injection gas; some runs were made with xenon in order to obtain a closer simulation of actual fission-gas properties. The number of this latter type of runs was kept rather small, however, because of the high cost of xenon.

Most test runs were performed with a needle internal diameter of 0.058 cm. Some were performed with needle internal diameters of 0.033 and 0.084 cm.

Nearly all runs were performed at ~50% of nominal power in order to extend the lifetime of the heaters. A series of test runs was performed at full power in order to ascertain that the temperature rise of the cladding in the affected pin-surface area is proportional with power.

For most runs, the coolant mass flow rate in the test section was ~690 g/sec. Some runs were made with smaller values for the coolant mass flow rate.

A limited number of test runs were made with a gas-plenum temperature T_g of 720°C as opposed to 510°C for most runs.

Figure 1 gives the temperature profile in the jet-impingement area for a gas-plenum pressure P_g = 7 bar (abs); from this figure, it is concluded that the impingement area extends axially over ~1.1 cm for the conditions pertaining to this test series. For gas-plenum pressures larger than 7 bar (abs), the maximum temperature rise is lower (see Figs. 2-8), and the impingement region is less well-defined, presumably because of the formation of coolant spray at the liquid-gas interface of the gas jet.[12,13]

A maximum cladding-temperature rise of ~120°C was measured at a heat flux of 126 W/cm^2 (see Fig. 9); noteworthy is the fact that the highest cladding-temperature rise occurred in a rather narrow range of values of the gas-plenum pressure, namely, for $P_g/P_s < \sim 3$, i.e., in the subsonic and

near-subsonic range. Earlier work regarding gas-jet impingement showed that, for $P_g/P_s > \sim 3$, considerable spray formation takes place at the gas-liquid interface of the gas jet, so that cooling in the impingement area is predominantly due to coolant spray.[1,8,9,13,14] For $P_g/P_s < \sim 3$, spray formation takes place to a lesser degree; it is postulated that under these latter conditions the cooling process depends mainly on the existence of a remaining coolant film, most of the coolant having been displaced from the subchannel by the gas. This latter phenomenon was first observed in an earlier experiment in which gas release in an LMFBR fuel subassembly was simulated by means of a 19-pin heated test section with water as coolant.[5]

Comparison of Figs. 9 and 10 shows that, as mentioned earlier, the cladding-temperature rise in the affected surface area is proportional to power, within the range of heat flux values tested; for a heat flux of 250 W/cm^2, a cladding-temperature rise of ~240°C was found (see Fig. 10).

Earlier data obtained in the sonic range of the gas jet showed that the magnitude of the coolant velocity has little or no effect on the cladding-temperature rise. This is understandable because (a) cooling depends primarily on the coolant spray formed at the liquid-gas interface of the gas jet and (b) the velocity of the coolant (maximum value ~8 m/sec) is very low if compared with the velocity in the sonic gas jet (~400 m/sec, depending on gas pressure and temperature), so that the coolant in the gas-jet region is virtually stagnant (even at its highest velocity) if compared with the gas in the jet. However, in the subsonic and near-subsonic range this is no longer true, since (1) coolant-spray formation may not take place or takes place to a lesser degree and (2) the velocity in the gas jet is smaller. Some effect of the magnitude of the coolant velocity on the cladding-temperature rise in the impingement area may thus be expected for subsonic and near-subsonic flow in the gas jet (see Figs. 11 and 12). The value of P_g/P_s for which the highest cladding-temperature rise occurs decreases for decreasing values of the coolant mass flow rate (see Figs. 9, 11, and 12). This phenomenon is attributable to the deflection of the gas jet by the coolant,[6,14] which decreases for decreasing values of the coolant velocity.

Figure 13 gives data obtained at low power and low flow; these test runs were performed to simulate fission-gas release in an LMFBR fuel subassembly at power and coolant flow values approximating those of decay-heat level and natural circulation at shutdown. It is noted that the measured cladding-temperature rises were small and well within the tolerable range, even for the conservative case of steady-state gas release.

As mentioned earlier, one test series was performed at a higher gas-plenum temperature than the others. Comparison of the data of Figs. 9 and 14, obtained for gas-plenum temperatures of, respectively, 510 and 720°C, indicates that the gas temperature has little or no effect on the cladding-temperature rise, at least for the operating conditions considered.

Figures 16-21 give data, obtained with needles with smaller (0.033 cm) and larger (0.084 cm) internal diameters than pertained to the test runs of Figs. 1-15. The use of these needles resulted, for argon, in lower values for the cladding-temperature rise than were obtained with the needle with an internal diameter of 0.058 cm. The value of P_g/P_s for which the highest cladding temperature rise occurred appeared to decrease for increasing values of the needle internal diameter (see Figs. 16, 9, and 21). It is believed that this phenomenon can be attributed to deflection of the gas jet by the coolant.[6,14] For small gas-jet diameters, the jet will reach the opposite pin only for sonic flow and for a certain minimum density of the gas (see Fig. 16); for large gas-jet diameters, subsonic flow with relatively low gas density is sufficient for the gas jet to reach the opposite pin (see Fig. 21). Figures 17-20 give, for an internal diameter of the needle of 0.084 cm, the cladding temperature rise versus the relative axial position Z of the gas-injection needle with respect to the internal thermocouples of the needle on which impingement took place. The curves of ΔT versus Z show a more pronounced peak for a needle internal diameter of 0.058 cm than for one of 0.084 cm (compare, for example, Figs. 1 and 17). The value of the needle internal diameter for which the highest cladding temperature rise in the impingement area occurs may depend on the ratio p/d of fuel-pin pitch and fuel-pin diameter, and could thus possibly be different for different fuel designs.

Figure 15 gives the results of a series of test runs in which xenon was used as fission-gas simulant. The maximum cladding temperature rise for the operating conditions tested occurred for xenon in approximately the same range of values of P_g/P_s as for argon, and was found to be ~80°C at a heat flux of 126 W/cm^2. Keep in mind, however, that for xenon the highest possible cladding-temperature rise does not necessarily occur for the same needle internal diameter and operating conditions as for argon. For the same values of P_g, T_g, and needle internal diameter, the ratios of the mass flow rates, $\dot{m}_{Xe}/\dot{m}_{Ar}$, and of the gas velocities, u_{Xe}/u_{Ar}, are for sonic flow of xenon and argon, respectively, 1.81 and 0.55. Thus, although the highest cladding-temperature rise measured for xenon extrapolated to 160°C at a heat flux of 250 W/cm^2, it appears prudent to assume, unless proof to the contrary is given, that a cladding-temperature rise of 240°C at a heat flux of 250 W/cm^2, as measured for argon, is also possible for xenon under operating conditions that differ slightly from those pertaining to Fig. 15.

As mentioned earlier, Figs. 22-42 give the heat-transfer coefficient, h*, in the impingement area during gas release between the external cladding surface temperature and the local bulk coolant temperature. In Appendix C the method followed for calculating h* from the cladding temperature rise and the operating conditions is discussed briefly.

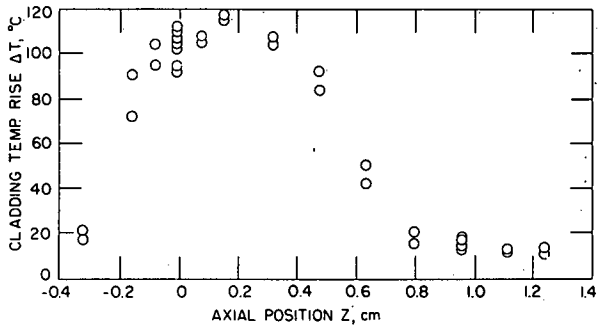

Fig. 1

Measured Cladding-temperature Rise, ΔT, in Impingement Area, as a Function of Relative Axial Position, Z, of Gas-release Needle with Respect to Internal Thermocouples of Heater Pin Impinged Upon, for Argon Gas with P_g = 7 bar (abs), T_g = 510°C, Needle ID = 0.058 cm, P_s = 4 bar (abs), q" = 126 W/cm^2, and $\dot{m}$ = 690 g/sec. ANL Neg. No. 900-2506 Rev. 2.

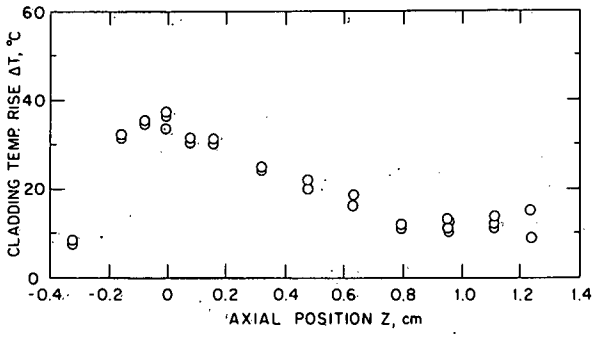

Fig. 2

Measured Cladding-temperature Rise, ΔT, in Impingement Area, as a Function of Relative Axial Position, Z, of Gas-release Needle with Respect to Internal Thermocouples of Heater Pin Impinged Upon, for Argon Gas with P_g = 14 bar (abs), T_g = 510°C, Needle ID = 0.058 cm, P_s = 4 bar (abs), q" = 126 W/cm^2, and $\dot{m}$ = 690 g/sec. ANL Neg. No. 900-2580 Rev. 1.

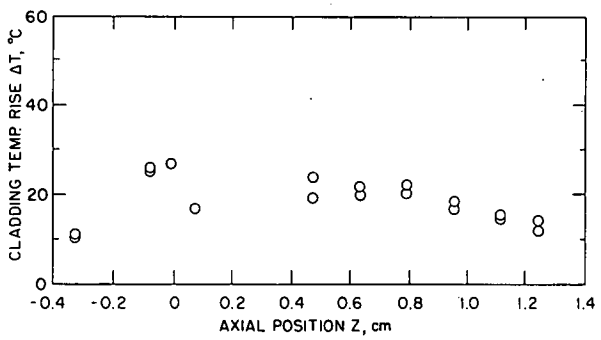

Fig. 3

Measured Cladding-temperature Rise, ΔT, in Impingement Area, as a Function of Relative Axial Position, Z, of Gas-release Needle with Respect to Internal Thermocouples of Heater Pin Impinged Upon, for Argon Gas with P_g = 21 bar (abs), T_g = 510°C, Needle ID = 0.058 cm, P_s = 4 bar (abs), q" = 126 W/cm^2, and $\dot{m}$ = 690 g/sec. ANL Neg. No. 900-2590 Rev. 1.

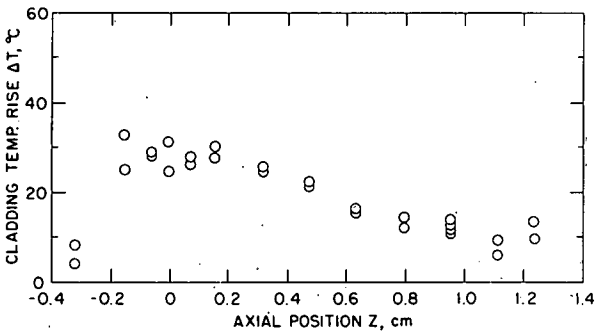

Fig. 4

Measured Cladding-temperature Rise, ΔT, in Impingement Area, as a Function of Relative Axial Position, Z, of Gas-release Needle with Respect to Internal Thermocouples of Heater Pin Impinged Upon, for Argon Gas with P_g = 28 bar (abs), T_g = 510°C, Needle ID = 0.058 cm, P_s = 4 bar (abs), q" = 126 W/cm^2, and $\dot{m}$ = 690 g/sec. ANL Neg. No. 900-2576 Rev. 1.

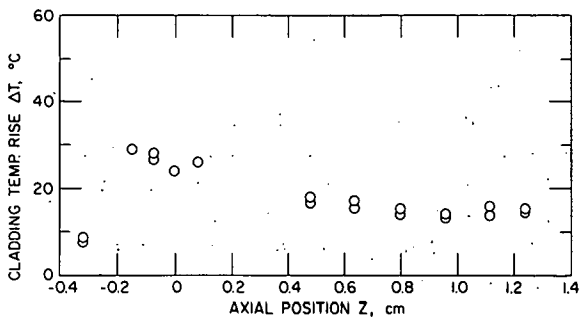

Fig. 5

Measured Cladding-temperature Rise, ΔT, in Impingement Area, as a Function of Relative Axial Position, Z, of Gas-release Needle with Respect to Internal Thermocouples of Heater Pin Impinged Upon, for Argon Gas with P_g = 35 bar (abs), T_g = 510°C, Needle ID = 0.058 cm, P_s = 4 bar (abs), q" = 126 W/cm^2, and $\dot{m}$ = 690 g/sec. ANL Neg. No. 900-2582 Rev. 1.

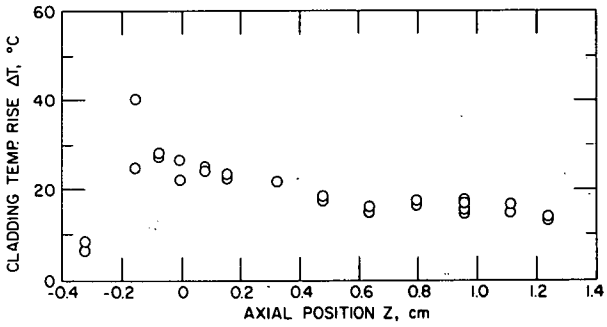

Fig. 6

Measured Cladding-temperature Rise, ΔT, in Impingement Area, as a Function of Relative Axial Position, Z, of Gas-release Needle with Respect to Internal Thermocouples of Heater Pin Impinged Upon, for Argon Gas with P_g = 41 bar (abs), T_g = 510°C, Needle ID = 0.058 cm, P_s = 4 bar (abs), q" = 126 W/cm^2, and $\dot{m}$ = 690 g/sec. ANL Neg. No. 900-2577 Rev. 1.

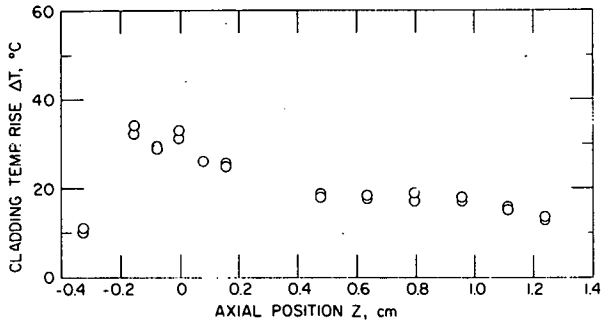

Fig. 7

Measured Cladding-temperature Rise, ΔT, in Impingement Area, as a Function of Relative Axial Position, Z, of Gas-release Needle with Respect to Internal Thermocouples of Heater Pin Impinged Upon, for Argon Gas with P_g = 48 bar (abs), T_g = 510°C, Needle ID = 0.058 cm, P_s = 4 bar (abs), q" = 126 W/cm^2, and $\dot{m}$ = 690 g/sec. ANL Neg. No. 900-2587 Rev. 1.

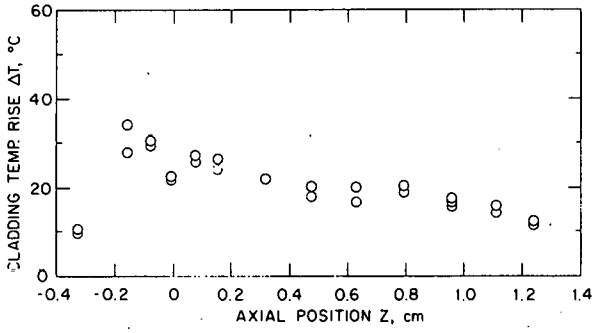

Fig. 8

Measured Cladding-temperature Rise, ΔT, in Impingement Area, as a Function of Relative Axial Position, Z, of Gas-release Needle with Respect to Internal Thermocouples of Heater Pin Impinged Upon, for Argon Gas with P_g = 54 bar (abs), T_g = 510°C, Needle ID = 0.058 cm, P_s = 4 bar (abs), q" = 126 W/cm^2, and $\dot{m}$ = 690 g/sec. ANL Neg. No. 900-2589 Rev. 1.

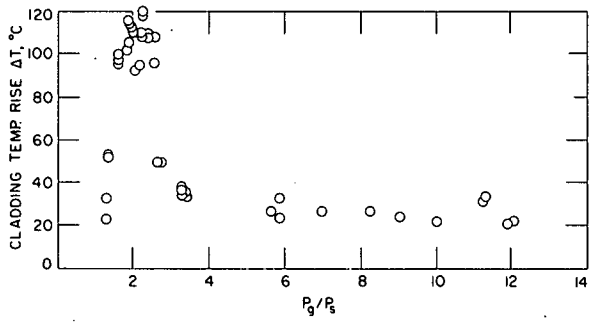

Fig. 9

Measured Cladding-temperature Rise, ΔT, in Impingement Area, as a Function of Ratio of Gas-plenum Pressure to System Coolant Pressure at Gas-release Point, P_g/P_s, for Argon Gas with T_g = 510°C, Needle ID = 0.058 cm, Z = 0, P_s = 4 bar (abs), q" = 126 W/cm^2, and $\dot{m}$ = 690 g/sec. ANL Neg. No. 900-2501 Rev. 3.

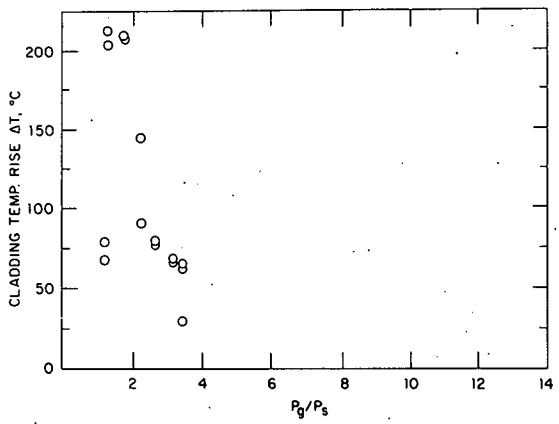

Fig. 10

Measured Cladding-temperature Rise, ΔT, in Impingement Area, as a Function of Ratio of Gas-plenum Pressure to system Coolant Pressure at Gas-release Point, P_g/P_s, for Argon Gas with T_g = 510°C, Needle ID = 0.058 cm, Z = 0, P_s = 4 bar (abs), q" = 250 W/cm^2, and $\dot{m}$ = 690 g/sec. ANL Neg. No. 900-2578 Rev. 1.

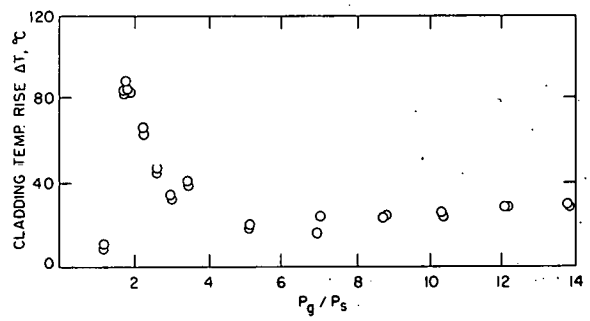

Fig. 11

Measured Cladding-temperature Rise, ΔT, in Impingement Area, as a Function of Ratio of Gas-plenum Pressure to System Coolant Pressure at Gas-release Point, P_g/P_s, for Argon Gas with T_g = 510°C, Needle ID = 0.058 cm, Z = 0, P_s = 4 bar (abs), q" = 126 W/cm^2, and $\dot{m}$ = 552 g/sec. ANL Neg. No. 900-2585 Rev. 1.

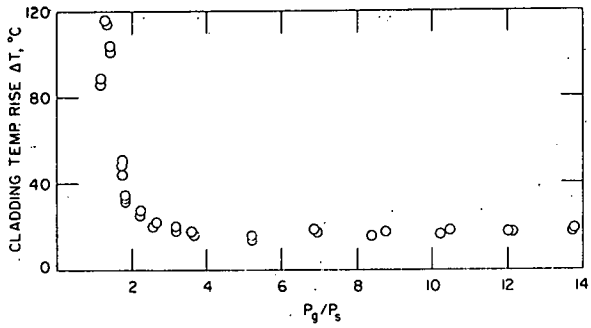

Fig. 12

Measured Cladding-temperature Rise, ΔT, in Impingement Area, as a Function of Ratio of Gas-plenum Pressure to System Coolant Pressure at Gas-release Point, P_g/P_s, for Argon Gas with T_g = 510°C, Needle ID = 0.058 cm, Z = 0, P_s = 4 bar (abs), q" = 126 W/cm^2, and $\dot{m}$ = 414 g/sec. ANL Neg. No. 900-2581 Rev. 1.

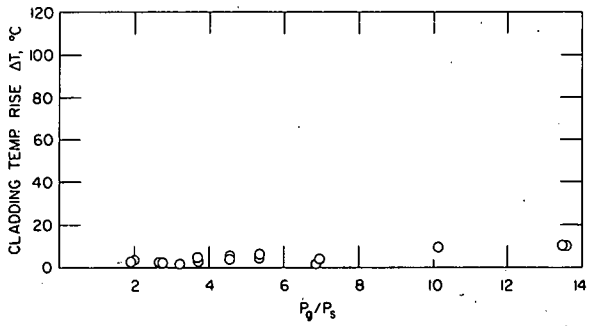

Fig. 13

Measured Cladding-temperature Rise, ΔT, in Impingement Area, as a Function of Ratio of Gas-plenum Pressure to System Coolant Pressure at Gas-release Point, P_g/P_s, for Argon Gas with T_g = 510°C, Needle ID = 0.058 cm, Z = 0, P_s = 4 bar (abs), q" = 25 W/cm^2, and $\dot{m}$ = 138 g/sec. ANL Neg. No. 900-2583 Rev. 1.

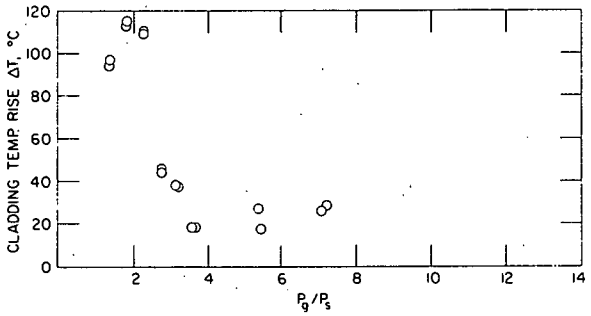

Fig. 14

Measured Cladding-temperature Rise, ΔT, in Impingement Area, as a Function of Ratio of Gas-plenum Pressure to System Coolant Pressure at Gas-release Point, P_g/P_s, for Argon Gas with T_g = 720°C, Needle ID = 0.058 cm, Z = 0, P_s = 4 bar (abs), q" = 126 W/cm^2, and $\dot{m}$ = 690 g/sec. ANL Neg. No. 900-2504 Rev. 2.

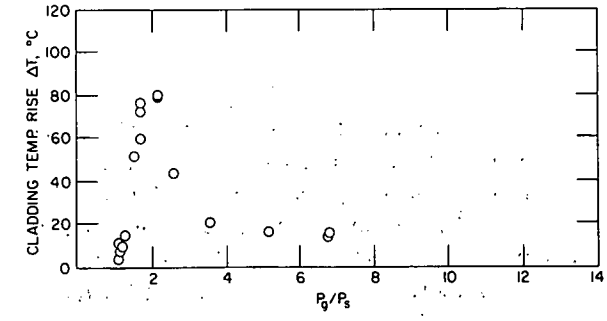

Fig. 15

Measured Cladding-temperature Rise, ΔT, in Impingement Area, as a Function of Ratio of Gas-plenum Pressure to System Coolant Pressure at Gas-release Point, P_g/P_s, for Xenon Gas with T_g = 510°C, Needle ID = 0.058 cm, Z = 0, P_s = 4 bar (abs), q" = 126 W/cm^2, and $\dot{m}$ = 690 g/sec. ANL Neg. No. 900-2502 Rev. 2.

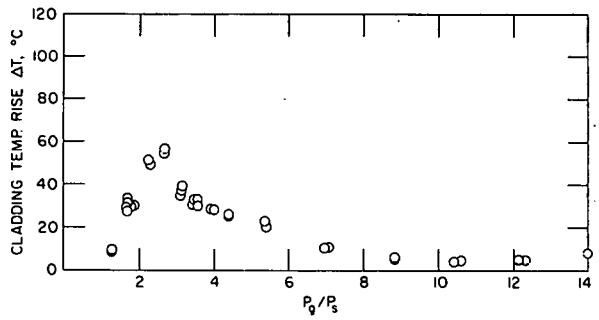

Fig. 16

Measured Cladding-temperature Rise, ΔT, in Impingement Area, as a Function of Ratio of Gas-plenum Pressure to System Coolant Pressure at Gas-release Point, P_g/P_s, for Argon Gas with T_g = 510°C, Needle ID = 0.033 cm, Z = 0, P_s = 4 bar (abs), q" = 126 W/cm^2, and $\dot{m}$ = 690 g/sec. ANL Neg. No. 900-2505 Rev. 2.

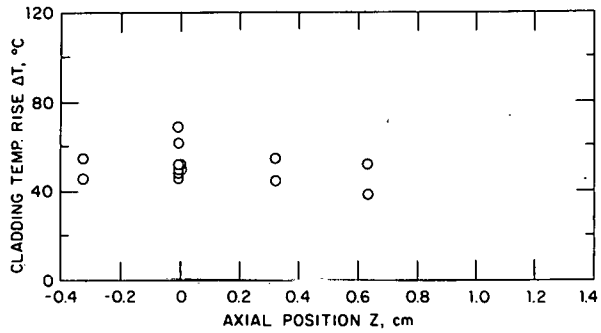

Fig. 17

Measured Cladding-temperature Rise, ΔT, in Impingement Area, as a Function of Relative Axial Position, Z, of Gas-release Needle with Respect to Internal Thermocouples of Heater Pin Impinged Upon, for Argon Gas with P_g = 7 bar (abs), T_g = 510°C, Needle ID = 0.084 cm, P_s = 4 bar (abs), q" = 126 W/cm^2, and $\dot{m}$ = 690 g/sec. ANL Neg. No. 900-2584 Rev. 2.

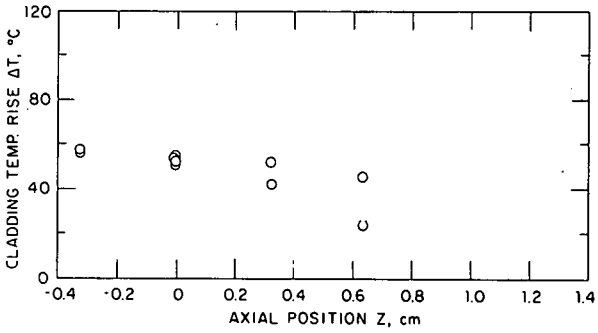

Fig. 18

Measured Cladding-temperature Rise, ΔT, in Impingement Area, as a Function of Relative Axial Position, Z, of Gas-release Needle with Respect to Internal Thermocouples of Heater Pin Impinged Upon, for Argon Gas with P_g = 10.5 bar (abs), T_g = 510°C, Needle ID = 0.084 cm, P_s = 4 bar (abs), q" = 126 W/cm^2, and $\dot{m}$ = 690 g/sec. ANL Neg. No. 900-2579 Rev. 2.

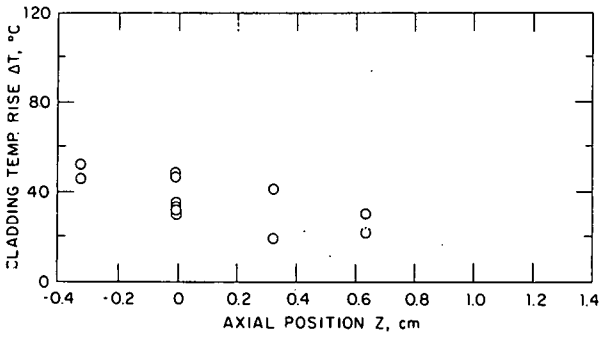

Fig. 19

Measured Cladding-temperature Rise, ΔT, in Impingement Area, as a Function of Relative Axial Position, Z, of Gas-release Needle with Respect to Internal Thermocouples of Heater Pin Impinged Upon, for Argon Gas with P_g = 14 bar (abs), T_g = 510°C, Needle ID = 0.084 cm, P_s = 4 bar (abs), q" = 126 W/cm^2, and $\dot{m}$ = 690 g/sec. ANL Neg. No. 900-2591 Rev. 2.

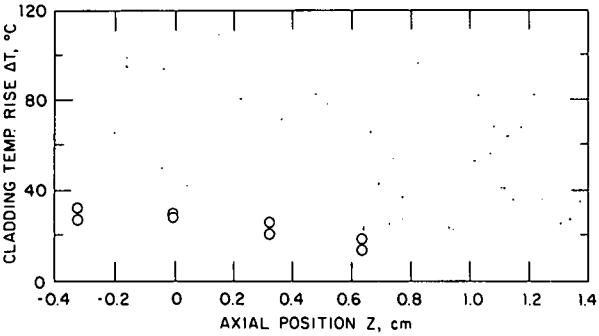

Fig. 20

Measured Cladding-temperature Rise, ΔT, in Impingement Area, as a Function of Relative Axial Position, Z, of Gas-release Needle with Respect to Internal Thermocouples of Heater Pin Impinged Upon, for Argon Gas with P_g = 17.5 bar (abs), T_g = 510°C, Needle ID = 0.084 cm, P_s = 4 bar (abs), q" = 126 W/cm^2, and $\dot{m}$ = 690 g/sec. ANL Neg. No. 900-2588 Rev. 2.

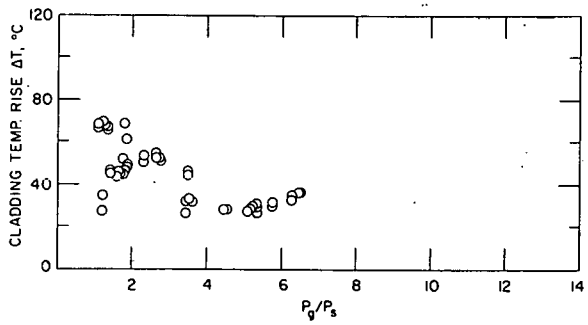

Fig. 21

Measured Cladding-temperature Rise, ΔT, in Impingement Area, as a Function of Ratio of Gas-plenum Pressure to System Coolant Pressure at Gas-release Point, P_g/P_s, for Argon Gas with T_g = 510°C, Needle ID = 0.084 cm, Z = 0, P_s = 4 bar (abs), q" = 126 W/cm^2, and $\dot{m}$ = 690 g/sec. ANL Neg. No. 900-2586 Rev. 1.

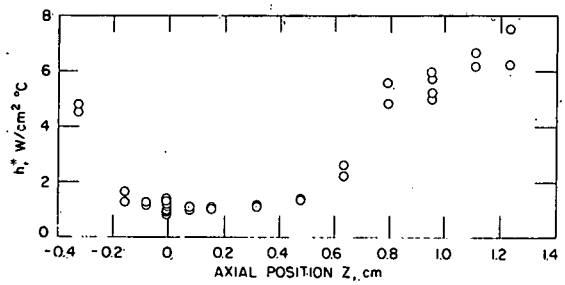

Fig. 22

Calculated Heat-transfer Coefficient, h*, in Impingement Area during Gas Release, as a Function of Relative Axial Position, Z, of Gas-release Needle with Respect to Internal Thermocouples of Heater Pin Impinged Upon, for Argon Gas with P_g = 7 bar (abs), T_g = 510°C, Needle ID = 0.058 cm, P_s = 4 bar (abs), q" = 126 W/cm^2, and $\dot{m}$ = 690 g/sec. ANL Neg. No. 900-2626 Rev. 1.

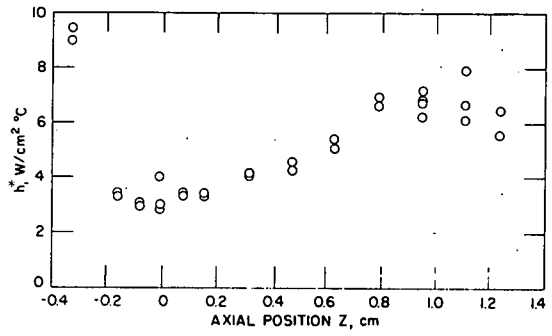

Fig. 23

Calculated Heat-transfer Coefficient, h*, in Impingement Area during Gas Release, as a Function of Relative Axial Position, Z, of Gas-release Needle with Respect to Internal Thermocouples of Heater Pin Impinged Upon, for Argon Gas with P_g = 14 bar (abs), T_g = 510°C, Needle ID = 0.058 cm, P_s = 4 bar (abs), q" = 126 W/cm^2, and $\dot{m}$ = 690 g/sec. ANL Neg. No. 900-2629 Rev. 1.

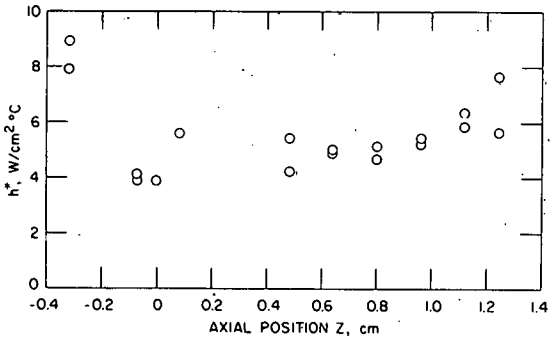

Fig. 24

Calculated Heat-transfer Coefficient, h*, in Impingement Area during Gas Release, as a Function of Relative Axial Position, Z, of Gas-release Needle with Respect to Internal Thermocouples of Heater Pin Impinged Upon, for Argon Gas with P_g = 21 bar (abs), T_g = 510°C, Needle ID = 0.058 cm, P_s = 4 bar (abs), q" = 126 W/cm^2, and $\dot{m}$ = 690 g/sec. ANL Neg. No. 900-2624 Rev. 1.

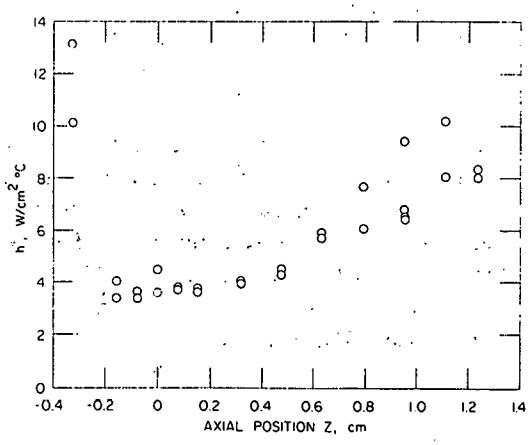

Fig. 25

Calculated Heat-transfer Coefficient, h*, in Impingement Area during Gas Release, as a Function of Relative Axial Position, Z, of Gas-release Needle with Respect to Internal Thermocouples of Heater Pin Impinged Upon, for Argon Gas with P_g = 28 bar (abs), T_g = 510°C, Needle ID = 0.058 cm, P_s = 4 bar (abs), q" = 126 W/cm^2, and $\dot{m}$ = 690 g/sec. ANL Neg. No. 900-2610 Rev. 1.

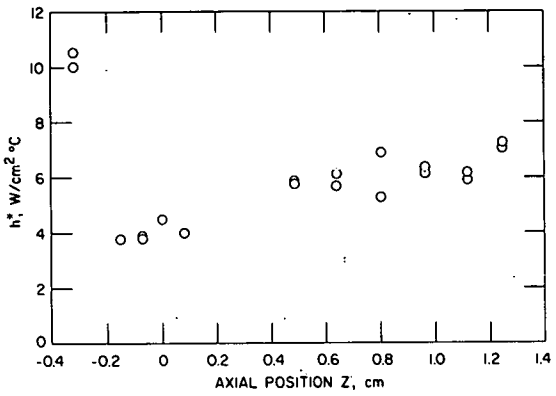

Fig. 26

Calculated Heat-transfer Coefficient, h*, in Impingement Area during Gas Release, as a Function of Relative Axial Position, Z, of Gas-release Needle with Respect to Internal Thermocouples of Heater Pin Impinged Upon, for Argon Gas with P_g = 35 bar (abs), T_g = 510°C, Needle ID = 0.058 cm, P_s = 4 bar (abs), q" = 126 W/cm^2, and $\dot{m}$ = 690 g/sec. ANL Neg. No. 900-2616 Rev. 1.

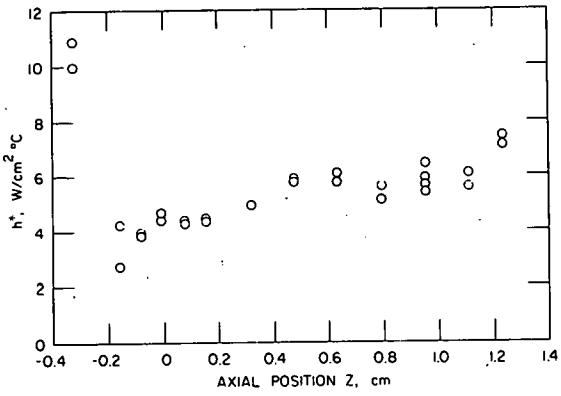

Fig. 27

Calculated Heat-transfer Coefficient, h*, in Impingement Area during Gas Release, as a Function of Relative Axial Position, Z, of Gas-release Needle with Respect to Internal Thermocouples of Heater Pin Impinged Upon, for Argon Gas with P_g = 41 bar (abs), T_g = 510°C, Needle ID = 0.058 cm, P_s = 4 bar (abs), q" = 126 W/cm^2, and $\dot{m}$ = 690 g/sec. ANL Neg. No. 900-2625 Rev. 1.

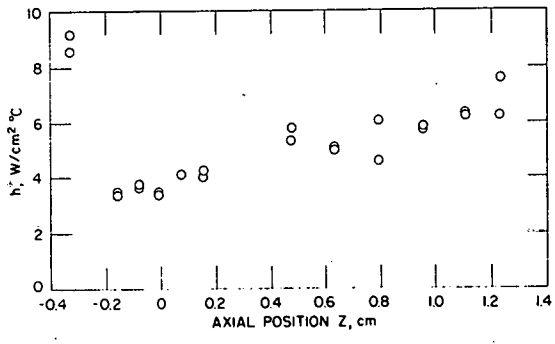

Fig. 28

Calculated Heat-transfer Coefficient, h*, in Impingement Area during Gas Release, as a Function of Relative Axial Position, Z, of Gas-release Needle with Respect to Internal Thermocouples of Heater Pin Impinged Upon, for Argon Gas with P_g = 48 bar (abs), T_g = 510°C, Needle ID = 0.058 cm, P_s = 4 bar (abs), q" = 126 W/cm^2, and $\dot{m}$ = 690 g/sec. ANL Neg. No. 900-2630 Rev. 1.

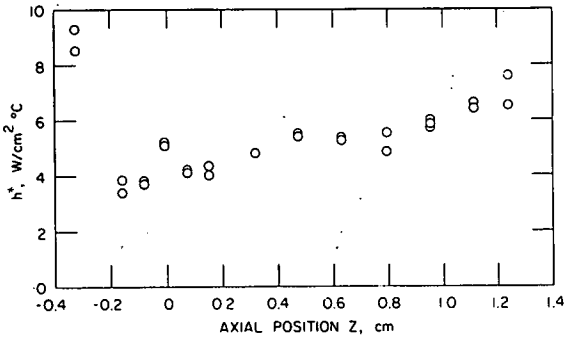

Fig. 29

Calculated Heat-transfer Coefficient, h*, in Impingement Area during Gas Release, as a Function of Relative Axial Position, Z, of Gas-release Needle with Respect to Internal Thermocouples of Heater Pin Impinged Upon, for Argon Gas with P_g = 54 bar (abs), T_g = 510°C, Needle ID = 0.058 cm, P_s = 4 bar (abs), q" = 126 W/cm^2, and $\dot{m}$ = 690 g/sec. ANL Neg. No. 900-2621 Rev. 1.

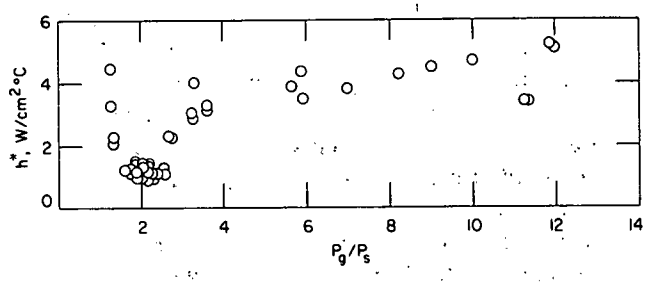

Fig. 30

Calculated Heat-transfer Coefficient, h*, in Impingement Area during Gas Release, as a Function of Ratio of Gas-plenum Pressure to System Coolant Pressure at Gas-release Point, P_g/P_s, for Argon Gas with T_g = 510°C, Needle ID = 0.058 cm, Z = 0, P_s = 4 bar (abs) q" = 126 W/cm^2, and $\dot{m}$ = 690 g/sec. ANL Neg. No. 900-2618 Rev. 1.

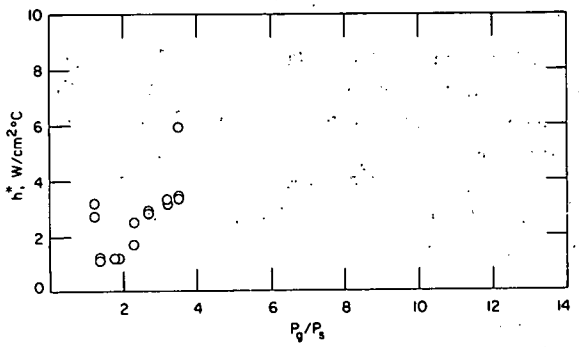

Fig. 31

Calculated Heat-transfer Coefficient, h*, in Impingement Area during Gas Release, as a Function of Ratio of Gas-plenum Pressure to System Coolant Pressure at Gas-release Point, P_g/P_s, for Argon Gas with T_g = 510°C, Needle ID = 0.058 cm, Z = 0, P_s = 4 bar (abs), q" = 250 W/cm^2, and $\dot{m}$ = 690 g/sec. ANL Neg. No. 900-2622 Rev. 1.

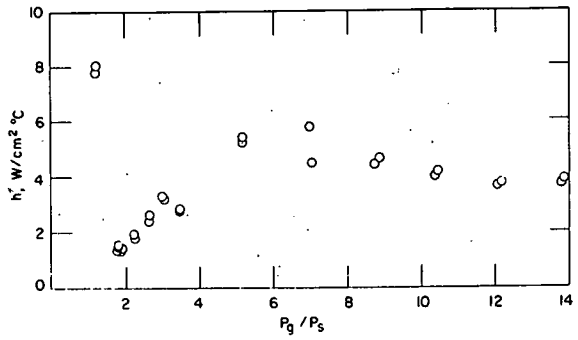

Fig. 32

Calculated Heat-transfer Coefficient, h*, in Impingement Area during Gas Release, as a Function of Ratio of Gas-plenum Pressure to System Coolant Pressure at Gas-release Point, P_g/P_s, for Argon Gas with T_g = 510°C, Needle ID = 0.058 cm, Z = 0, P_s = 4 bar (abs), q" = 126 W/cm^2, and $\dot{m}$ = 552 g/sec. ANL Neg. No. 900-2628 Rev. 1.

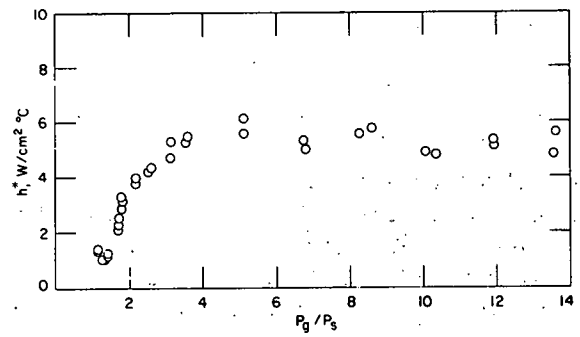

Fig. 33

Calculated Heat-transfer Coefficient, h*, in Impingement Area during Gas Release, as a Function of Ratio of Gas-plenum Pressure to System Coolant Pressure at Gas-release Point, P_g/P_s, for Argon Gas with T_g = 510°C, Needle ID = 0.058 cm, Z = 0, P_s = 4 bar (abs), q" = 126 W/cm^2, and $\dot{m}$ = 414 g/sec. ANL Neg. No. 900-2611 Rev. 1.

Fig. 34

Calculated Heat-transfer Coefficient, h*, in Impingement Area during Gas Release, as a Function of Ratio of Gas-plenum Pressure to System Coolant Pressure at Gas-release Point, P_g/P_s, for Argon Gas with T_g = 510°C, Needle ID = 0.058 cm, Z = 0, P_s = 4 bar (abs), q" = 25 W/cm^2, and $\dot{m}$ = 138 g/sec. ANL Neg. No. 900-2613 Rev. 1.

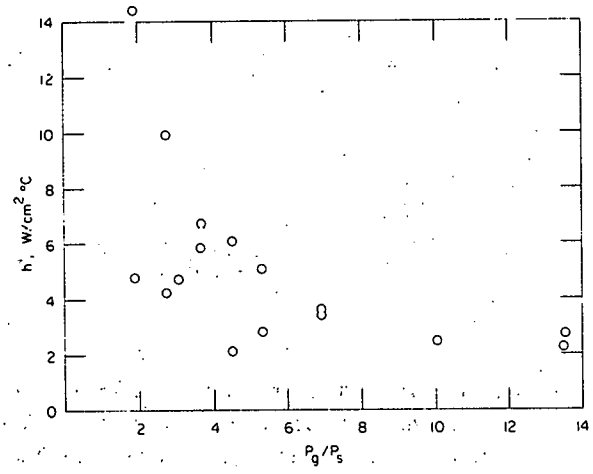

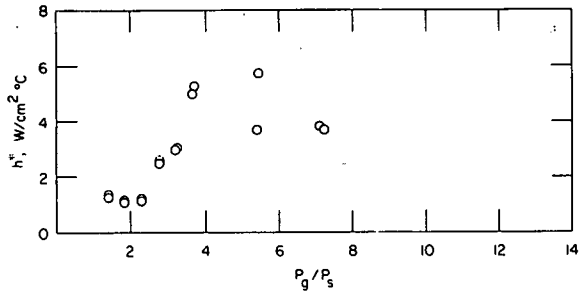

Fig. 35

Calculated Heat-transfer Coefficient, h*, in Impingement Area during Gas Release, as a Function of Ratio of Gas-plenum Pressure to System Coolant Pressure at Gas-release Point, P_g/P_s, for Argon Gas with T_g = 720°C, Needle ID = 0.058 cm, Z = 0, P_s = 4 bar (abs), q" = 126 W/cm^2, and $\dot{m}$ = 690 g/sec. ANL Neg. No. 900-2612 Rev. 1.

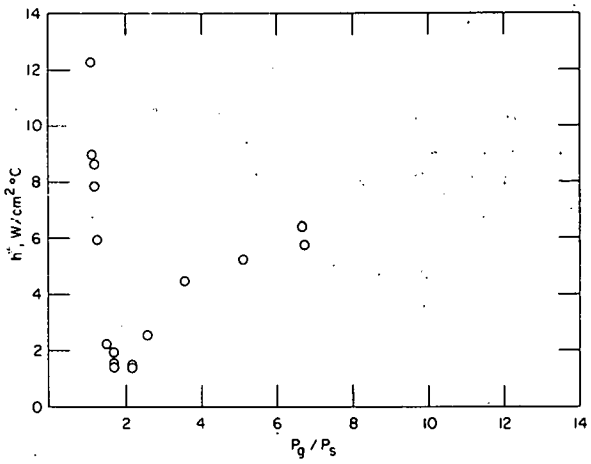

Fig. 36

Calculated Heat-transfer Coefficient, h*, in Impingement Area during Gas Release, as a Function of Ratio of Gas-plenum Pressure to System Coolant Pressure at Gas-release Point, P_g/P_s, for Xenon Gas with T_g = 510°C, Needle ID = 0.058 cm, Z = 0, P_s = 4 bar (abs), q" = 126 W/cm^2, and $\dot{m}$ = 690 g/sec. ANL Neg. No. 900-2615 Rev. 1.

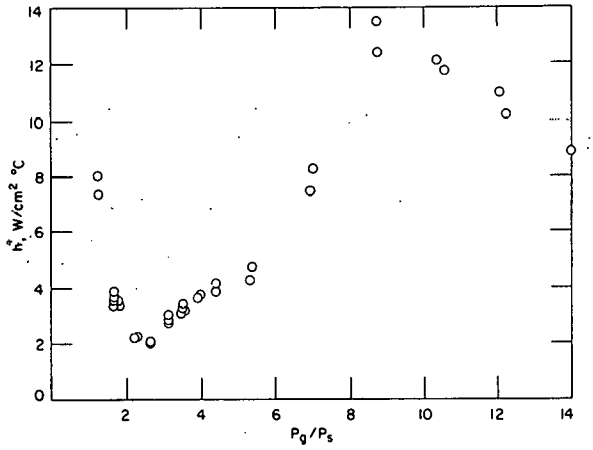

Fig. 37

Calculated Heat-transfer Coefficient, h*, in Impingement Area during Gas Release, as a Function of Ratio of Gas-plenum Pressure to System Coolant Pressure at Gas-release Point, P_g/P_s, for Argon Gas with T_g = 510°C, Needle ID = 0.033 cm, Z = 0, P_s = 4 bar (abs), q" = 126 W/cm^2, and $\dot{m}$ = 690 g/sec. ANL Neg. No. 900-2619 Rev. 2.

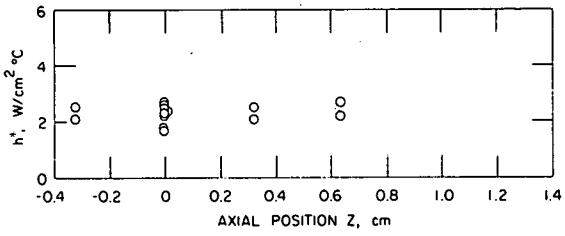

Fig. 38

Calculated Heat-transfer Coefficient, h*, in Impingement Area during Gas Release, as a Function of Relative Axial Position, Z, of Gas-release Needle with Respect to Internal Thermocouples of Heater Pin Impinged Upon, for Argon Gas with P_g = 7 bar (abs), T_g = 510°C, Needle ID = 0.084 cm, P_s = 4 bar (abs), q" = 126 W/cm^2, and $\dot{m}$ = 690 g/sec. ANL Neg. No. 900-2614 Rev. 1.

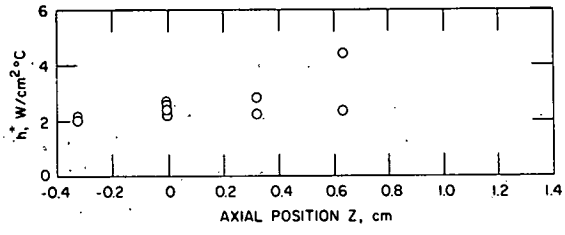

Fig. 39

Calculated Heat-transfer Coefficient, h*, in Impingement Area during Gas Release, as a Function of Relative Axial Position, Z, of Gas-release Needle with Respect to Internal Thermocouples of Heater Pin Impinged Upon, for Argon Gas with P_g = 10.5 bar (abs), T_g = 510°C, Needle ID = 0.084 cm, P_s = 4 bar (abs), q" = 126 W/cm^2, and $\dot{m}$ = 690 g/sec. ANL Neg. No. 900-2617 Rev. 1.

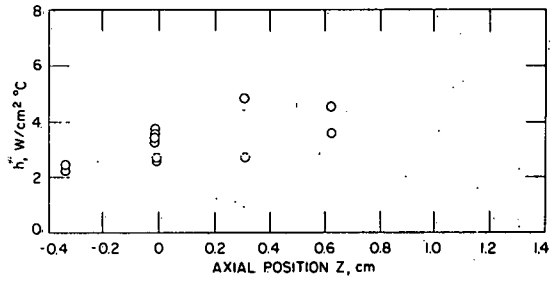

Fig. 40

Calculated Heat-transfer Coefficient, h*, in Impingement Area during Gas Release, as a Function of Relative Axial Position, Z, of Gas-release Needle with Respect to Internal Thermocouples of Heater Pin Impinged Upon, for Argon Gas with P_g = 14 bar (abs), T_g = 510°C, Needle ID = 0.084 cm, P_s = 4 bar (abs), q" = 126 W/cm^2, and $\dot{m}$ = 690 g/sec. ANL Neg. No. 900-2627 Rev. 1.

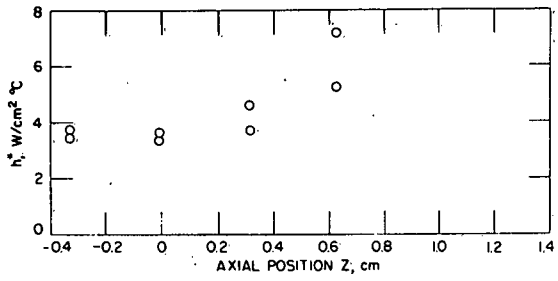

Fig. 41

Calculated Heat-transfer Coefficient, h*, in Impingement Area during Gas Release, as a Function of Relative Axial Position, Z, of Gas-release Needle with Respect to Internal Thermocouples of Heater Pin Impinged Upon, for Argon Gas with P_g = 17.5 bar (abs), T_g = 510°C, Needle ID = 0.084 cm, P_s = 4 bar (abs), q" = 126 W/cm^2, and $\dot{m}$ = 690 g/sec. ANL Neg. No. 900-2623 Rev. 1.

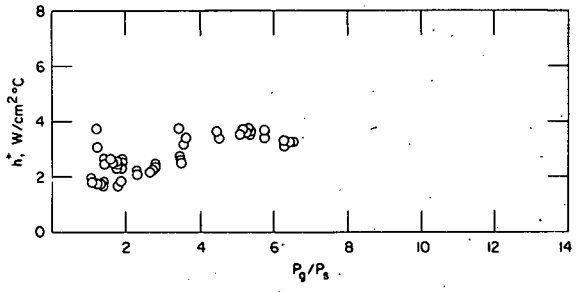

Fig. 42

Calculated Heat-transfer Coefficient, h*, in Impingement Area during Gas Release, as a Function of Ratio of Gas-plenum Pressure to System Coolant Pressure at Gas-release Point, P_g/P_s, for Argon Gas with T_g = 510°C, Needle ID = 0.084 cm, Z = 0, P_s = 4 bar (abs), q" = 126 W/cm^2, and $\dot{m}$ = 690 g/sec. ANL Neg. No. 900-2620 Rev. 1.

IV. SUMMARY AND CONCLUSIONS

1. Gas-jet impingement using argon to simulate fission gas was found to result, within a narrow range of gas flow rates at subsonic and near-subsonic conditions with $P_g/P_s < \sim 3$, in cladding-temperature rises in the impingement area of up to ~240°C at a heat flux of 250 W/cm^2.

2. The gas-jet impingement area was found to extend axial over a distance of ~1.1 cm when argon was used to simulate fission gas and P_g = 7 bar (abs); for $P_g > 7$ bar (abs), the impingement area was found to be less well-defined.

3. The use of xenon for simulating fission gas resulted qualitatively in the same results as obtained with argon. At subsonic and near-subsonic conditions with $P_g/P_s < \sim 3$, release of xenon resulted in cladding-temperature rises that extrapolated to ~160°C at a heat flux of 250 W/cm^2. It is believed, however, that release of xenon could, under slightly different operating conditions as those for which the tests were run, result in cladding temperature rises of approximately equal magnitude as those found for argon.

4. For $P_g/P_s > \sim 3$, coolant velocity has little or no effect on the cladding-temperature rise in the impingement area; for $P_g/P_s < \sim 3$, the cladding-temperature rise is affected to some degree by the value of the coolant velocity.

5. For low-power and low-flow conditions, approximating decay-heat power level and natural coolant circulation, the measured cladding temperature rises in the gas-jet impingement area are small and well within tolerable limits.

6. Gas-plenum temperature T_g was found to have, within the range of values tested, little direct effect on the cladding temperature rise in the gas-jet impingement area, in that:

   a. For $P_g/P_s > \sim 3$, spray cooling was predominant.

   b. For $P_g/P_s < \sim 3$, film cooling was predominant.

7. Test runs using gas-injection needles with various values of the internal diameter appear to indicate that a maximum value of the cladding-temperature rise in the impingement area occurred for an internal diameter of ~0.058 cm. This latter value may depend on the ratio p/d of fuel-pin pitch and fuel-pin diameter, and could thus be different for different fuel designs.

8. The data clearly indicate that gas-jet deflection by the coolant increases, as expected, for:

   a. Increasing values of the coolant velocity.

   b. Decreasing values of the gas-jet diameter (at constant gas velocity).

   c. Decreasing values of the density in the gas jet.

APPENDIX A

Description of Test Section

Figure A.1 is a schematic representation of the test section and includes a number of cross sections at various axial locations. Three uniformly electrically heated pins (of 0.584-cm OD) were arranged in an equilateral triangular configuration surrounded by a triflute shroud, which in turn was surrounded by a cylindrical pressure chamber. Wire spacers (of 0.157-cm OD), wrapped around the heaters at a pitch of 30.5 cm, were used for spacing the heater pins. The wire wraps, each of which had seven internal thermocouples spaced axially 7.6 cm apart, were spotwelded onto the heaters at 5-cm intervals to prevent movement. Additional spacers were installed over a short length in the inlet region of the test section (see Fig. A.2) in order to provide positive location of the heater pins within the triflute. The heaters, which entered the test section from the top through Swagelok fittings (see Fig. A.3) for easy replacement, consisted of a Nichrome electrical-resistance heater cartridge insulated from the stainless steel outer sheath by boron nitride and were provided with internal thermocouples (see Fig. A.4). These internal thermocouples were spotwelded at the junction onto the inside of the heater sheath and were axially located 18.2 cm downstream from the test-section inlet. The angular orientation of the heaters was such that the internal thermocouples faced the central coolant subchannel (see Fig. A.5). The total cross-sectional area for flow of the test section was 1.476 cm^2.

Argon or xenon was released from needles (of 0.033, 0.058, and 0.084-cm ID) protruding through the test-section pressure chamber and the triflute shroud between two heaters (see Fig. A.5). The end of the needles were, for all test runs, adjusted to be at a distance of ~0.142 cm (i.e., equal to the minimum distance between fuel pins in a fuel subassembly of the Fast Flux Test Facility--FFTF) from the heater pin to be impinged upon. The gas for all test runs was preheated by means of a gas-heating and -control system (see Fig. A.6). The heater pin to be impinged upon could be moved axially, since it was mounted by means of a bellows at the top of the test section; a device, consisting of a rack-and-pinion with jackscrew and driven by an electrical motor, permitted adjustment of the axial position of this heater from the control panel, so that the location of the gas jet could be varied with respect to the internal thermocouples. A potentiometer was used for accurate readout and recording of position (see Figs. A.7 and A.8). In this way an axial temperature profile of the impingement area could be obtained.

The tests were performed at steady state to eliminate the effects of flow and temperature transients. The testing procedure was as follows: (a) Gas was released at a predetermined constant rate; (b) the pump head was adjusted to maintain constant flow; (c) temperature readings were taken after reaching new steady-state conditions.

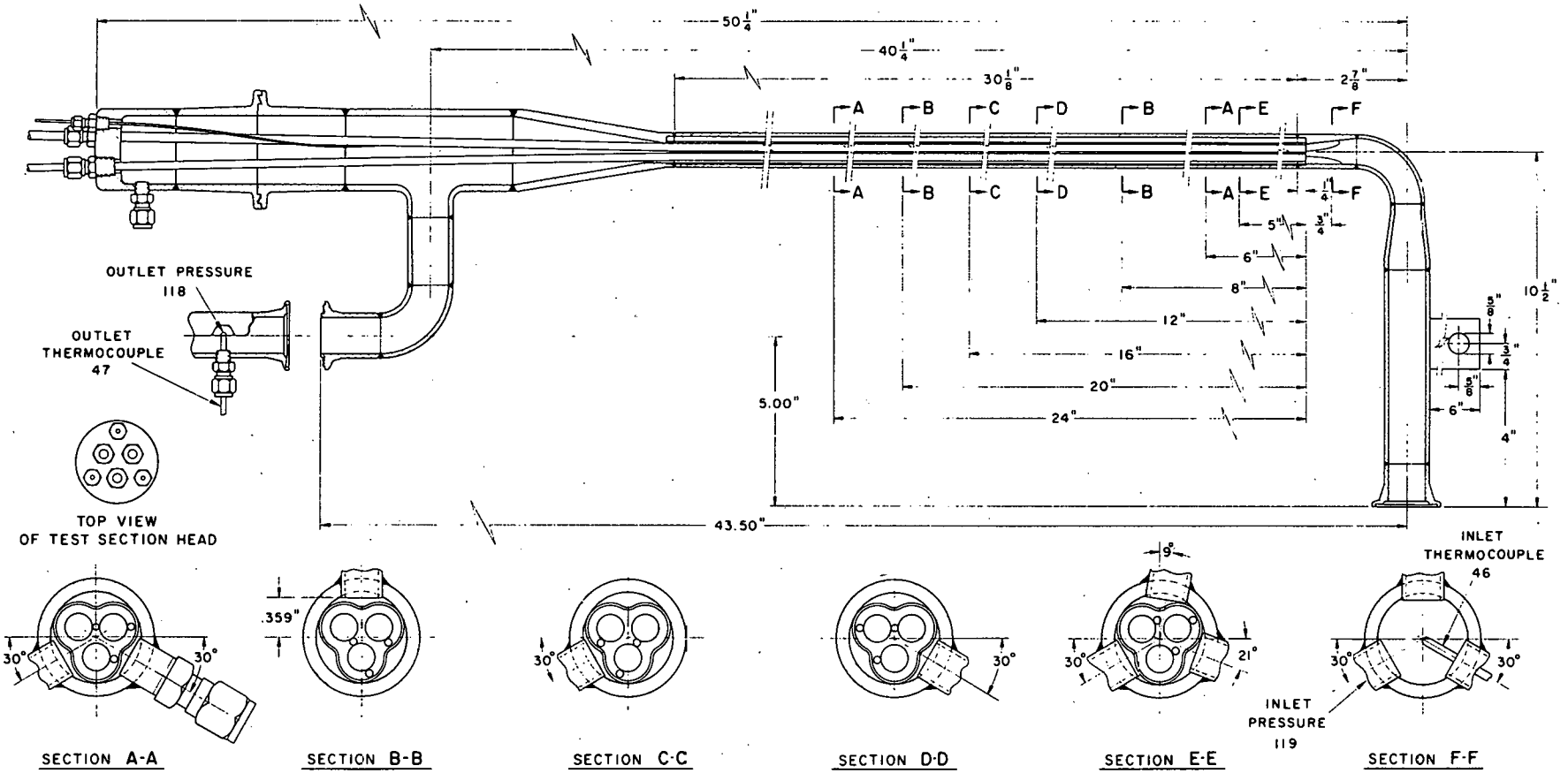

Fig. A.1. Schematic Representation of Three-pin Sodium Test Section. ANL Neg. No. 900-1331.

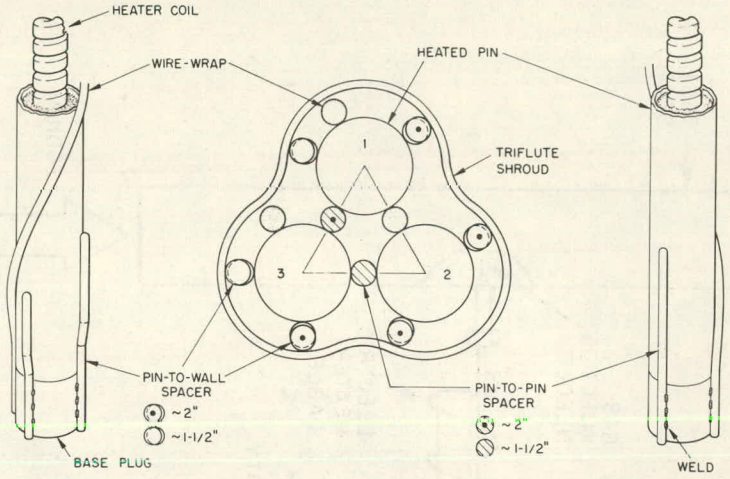

Fig. A.2. Cross Section of Three-pin Test Section, Showing Pin-to-Wall and Pin-to-Pin Spacers. ANL Neg. No. 900-2632.

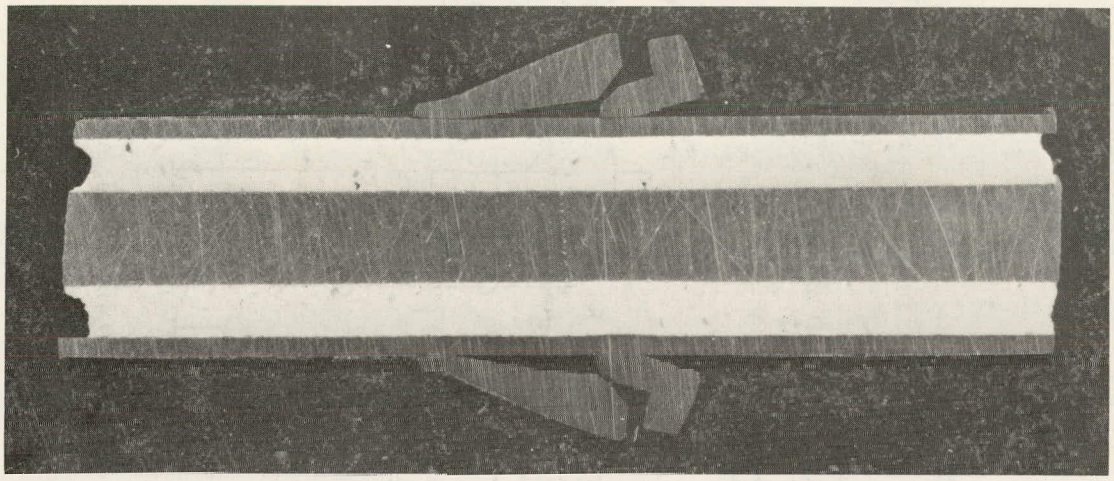

Fig. A.3. Lengthwise Section of Heater, with Swagelok Fitting for Installation in Top Portion of Test Section. ANL Neg. No. 900-1462.

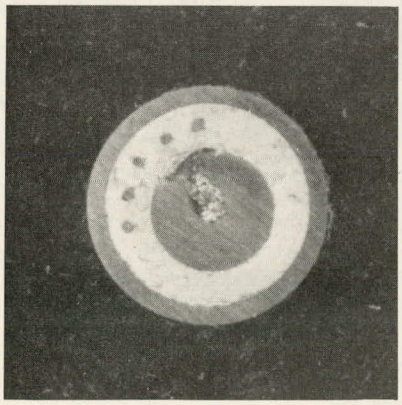

Fig. A.4. Cross Section of Heater, Showing Five Thermoelements. ANL Neg. No. 900-1463.

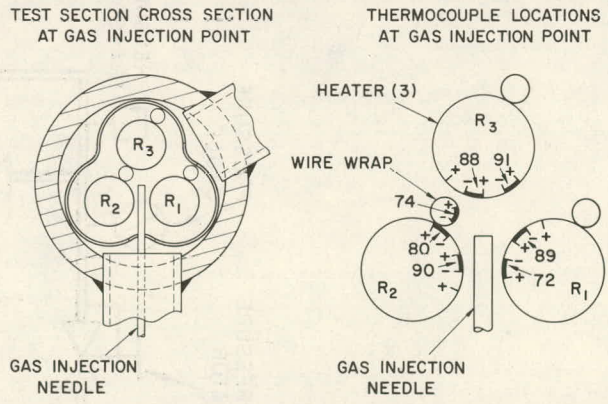

Fig. A.5. Schematic Representation of Cross Section of Three-pin Test Section at Gas-injection Point. Thermocouples inside the heaters are numbered 72, 80, 88, 89, 90, and 91; thermocouple inside the wire wrap is numbered 74. ANL Neg. No. 900-1333.

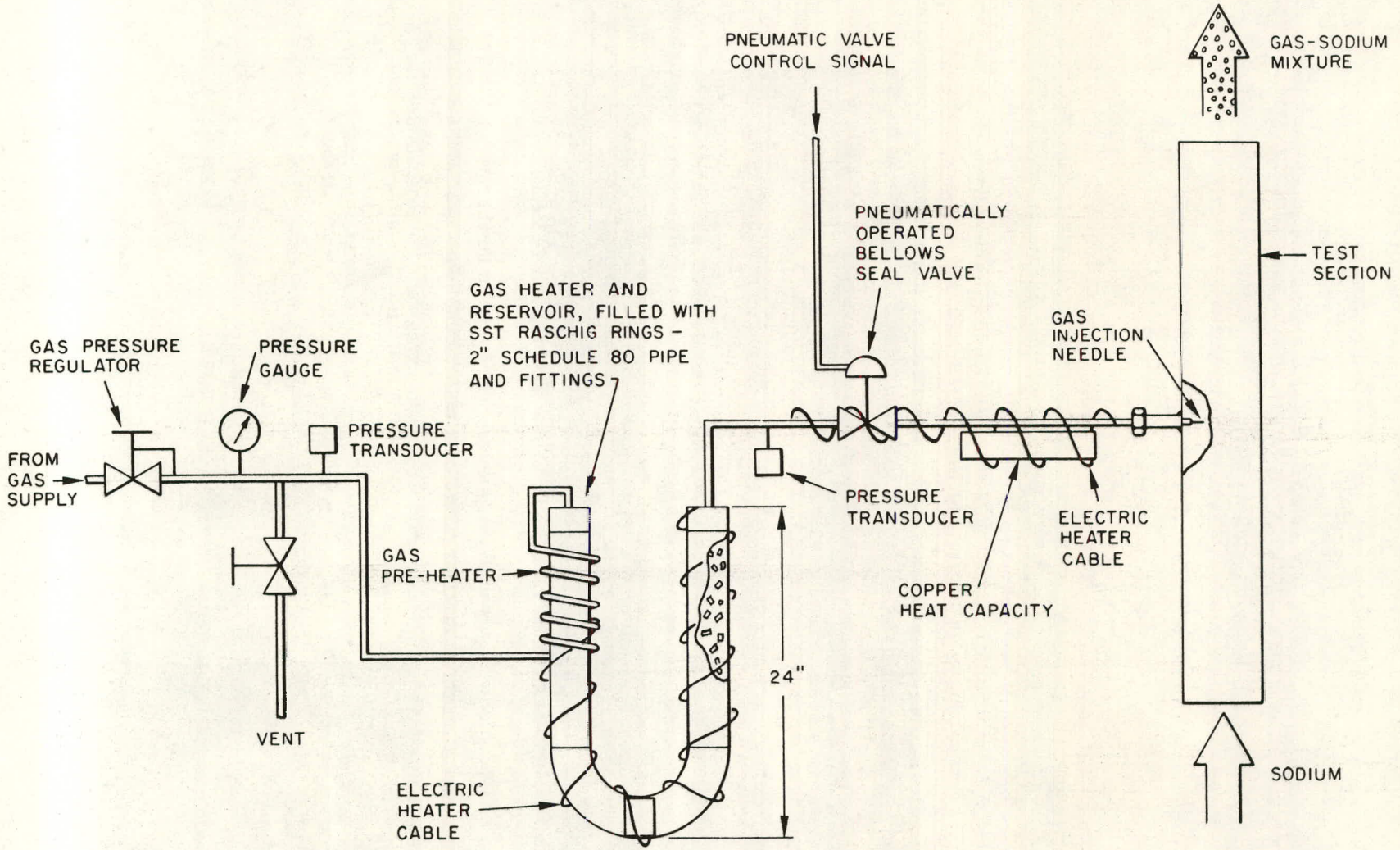

Fig. A.6. Gas-control and -heating System. ANL Neg. No. 900-2631.

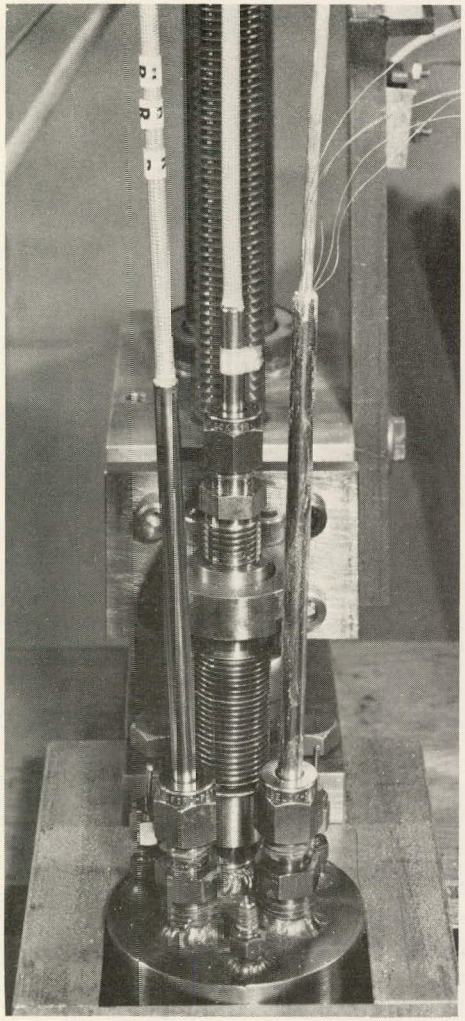

Fig. A.7. Top Portion of Three-pin Test Section, Showing Bellows for Movable Heater Pin, and Swagelok Fittings for Heaters and Wire Wraps. ANL Neg. No. 900-1472.

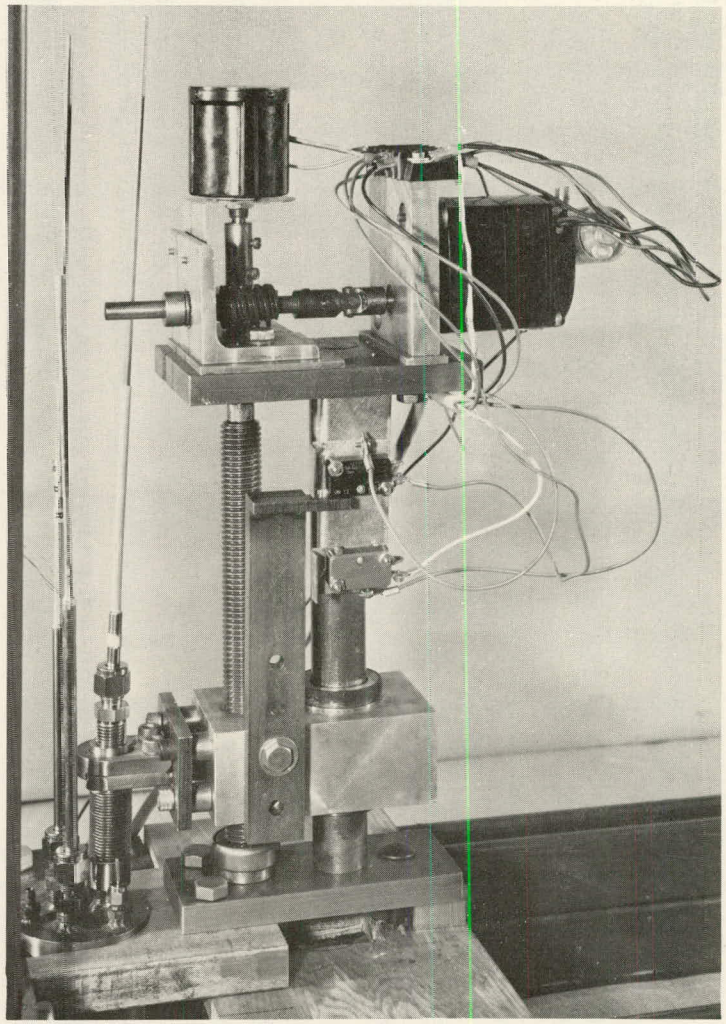

Fig. A.8. Top Portion of Three-pin Test Section Showing Rack-and-Pinion and Jackscrew Arrangements for Movable Heater Pin. ANL Neg. No. 900-1473.

APPENDIX B

Description of Sodium Loop

The sodium loop used for the experiments consisted of the following main components: a dump tank, an electromagnetic pump, a heat exchanger, and a test section (see Figs. B.1 and B.2). The main piping was 1-in. Schedule 40, Type 304 stainless steel. The piping system was welded, except for the test section, which was installed with Conoseal couplings to permit easy replacement.

The electromagnetic pump was rated 50 gpm at a head of 100 psi; 80 psi remained available for the pressure drop in the test section. Components are on hand to increase the loop to 2-in. pipe, thus allowing for higher flows. The sodium flow rate through the main loop was measured by means of magnetic flowmeters.

A combination dump and charging tank, having a 25-gal capacity, was installed at the lowest point of the loop. The total sodium holdup in the entire loop system was about 15 gal. Approximately 20 gal of sodium was normally charged to the tank to provide an excess heel in which impurities could settle out of the sodium. The tank was equipped with high- and low-level probes, and a well for subsequent use of an induction-type level probe. The dump valve was a manually operated 1-in. IPS bellows seal globe valve. The loop was normally operated with this valve open, the sodium being held by an electrically controlled freeze plug. A small surge tank of about 1-gal capacity was installed at the highest point in the system. This tank was equipped with a high-level probe. In addition, both the dump tank and the surge tank were connected to an argon blanket system. To prevent plugging of the argon lines with condensed sodium, connections to the tanks were made through sodium-vapor traps.

The air-cooled heat exchanger was designed to remove 10^6 Btu/hr from 204 lb/min of sodium which enters at 1075°F and leaves at 775°F. The coolant air enters at about 80°F, flows parallel to the tubes, and discharges at about 350°F. With a heat capacity of air of 0.25 Btu/lb-°F, the requirements for coolant-airflow are 246 lb/min or ~320 cu ft/min at the inlet end. The heat exchanger contains 24 horizontal tubes arranged in six parallel sets with four tubes in each set. The tubes are connected to manifolds at the inlet and outlet, and each set contains three 180° return bends. Since the direction of sodium flow in the tubes reverses at each 180° bend, the sodium and coolant air do not follow a true countercurrent flow pattern, and an average ΔT of 700°F was used for heat-transfer calculations. The 24 tubes are 1-in. OD x 0.143-in. wall, Type 304 seamless stainless steel. Each tube has 20 longitudinal fins, 6 ft long, 1/2 in. high, and 0.035 in. thick. Overall fin efficiency was estimated to be 50%, giving an effective heat-transfer surface of 1 sq ft per foot of tube length. The tubes are arranged in a rectangular array on 3 x 3-in. centers (with a slight pitch toward the outlet end to facilitate draining). To increase the air velocity around the finned tubes,

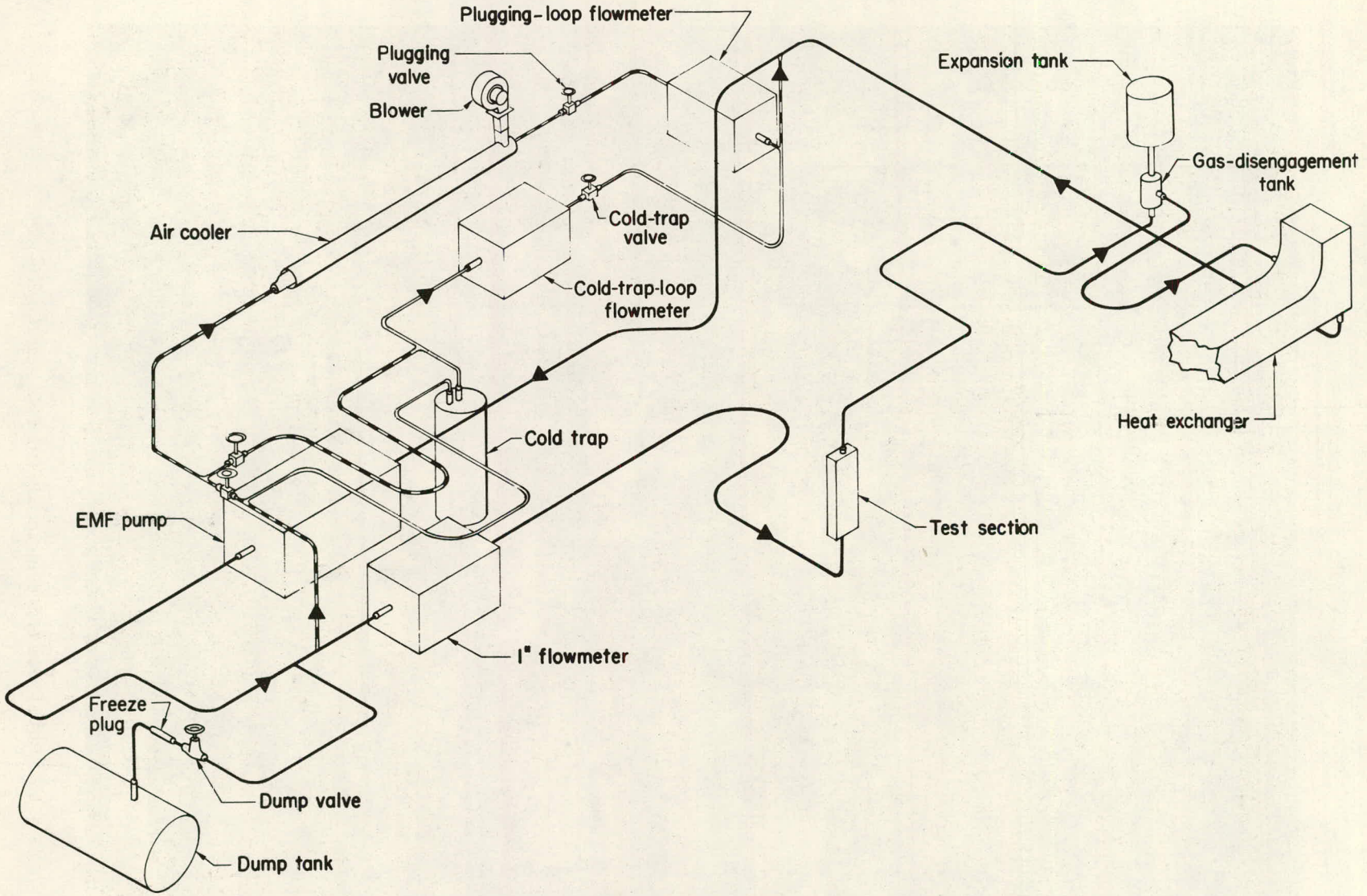

Fig. B.1. Schematic Representation of Sodium Loop. ANL Neg. No. 900-829.

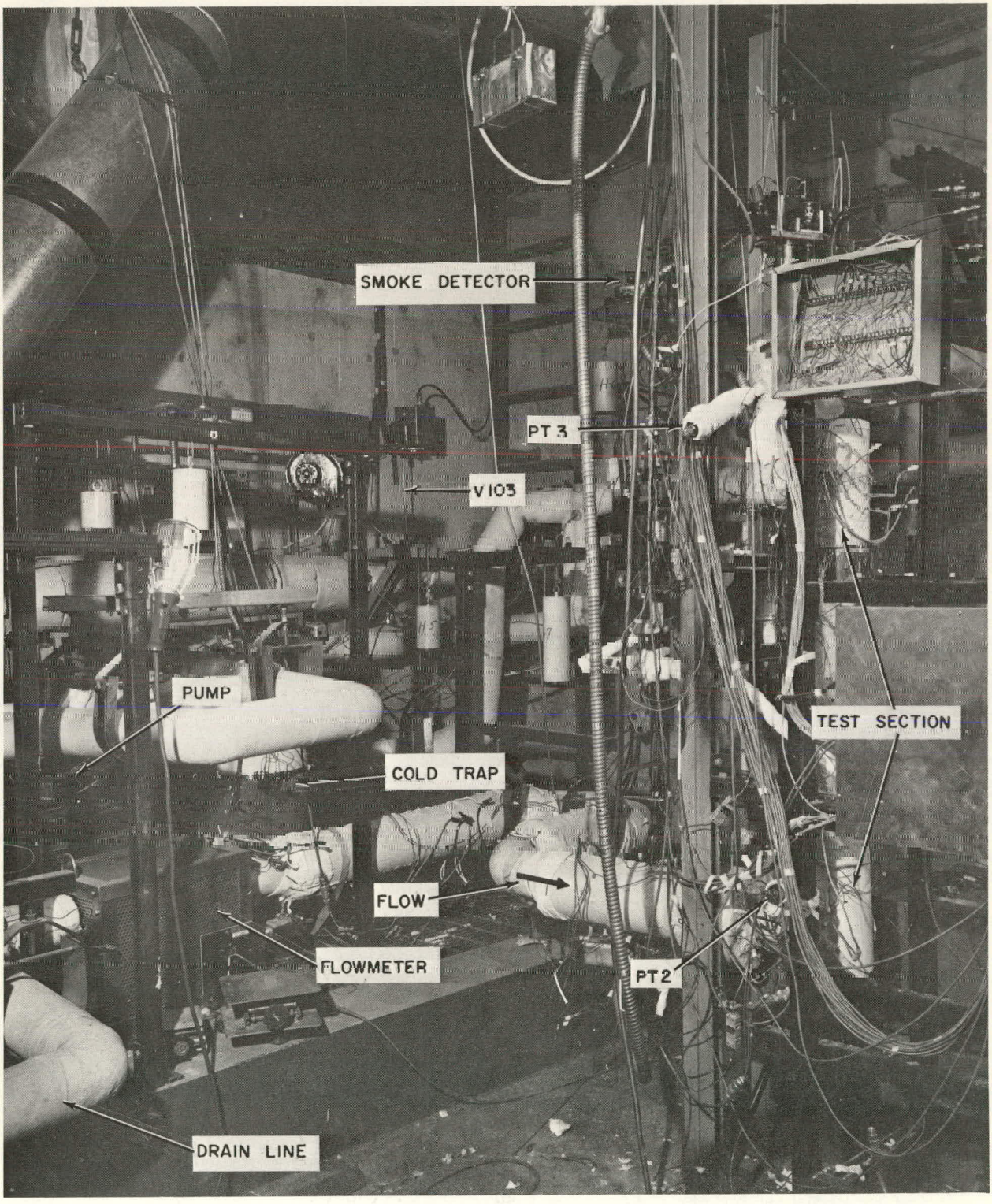

Fig. B.2. Partial View of Sodium Loop in Pit. ANL Neg. No. 900-1930.

15 dummy tubes, of $1\frac{3}{4}$-in. OD, are positioned in the void spaces between the finned tubes. The net free airflow area is 1.23 sq ft, resulting in air velocity of 43 ft/sec at the inlet end. Under these conditions, an overall heat-transfer coefficient of 10 Btu/hr-ft^2-°F can reasonably be expected. The heat-transfer surface required is 143 sq ft. The 24 finned tubes, each 6 ft long, provide the equivalent of 144 sq ft of surface. If necessary, increased heat-removal capability can be obtained by increasing the air-blower output. Coolant air is supplied to the heat exchanger by a centrifugal fan equipped with a 7.5-hp motor that can deliver up to 4000 cfm against 4 in. of water static pressure. A motorized damper in the air duct to the heat-exchanger plenum is manually controlled to regulate the airflow.

The secondary loop system contained a sodium cold trap and plugging valve. The pipe lines are 3/8-in. IPS Schedule 40, and the valves are 3/8-in. IPS manually operated bellows seal globe valves. The cold trap is 24 in. high and 6 in. in diameter, with a holdup capacity of about 3 gal. A 4-in.-dia tube, located concentrically within the 6-in.-dia tube, provides for an outer annulus through which the hot sodium flows downward and an inner tube through which the cold sodium flows upward. The two concentric zones thus provide for heat exchange between the inlet and outlet sodium. The outer tube is surrounded by a spiral air duct through which coolant air is blown from bottom to top. The cold trap is designed to operate at a flow rate of 0.5 gal/min of sodium entering at 800°F and leaving at 650°F. A minimum sodium temperature of about 250°F is expected to be reached at the bottom of the trap when approximately 60 cfm of coolant air is flowing through the air duct. Both the annular sodium-flow zone and the 4-in.-dia inner tube are packed with stainless steel wool for collection of precipitated oxide. The parallel section of the secondary loop contains the plugging valve. The plugging valve itself is a modified globe valve in which small slots were machined in the valve-stem adapter to provide a set of fine orifices for collecting precipitated oxide. The system has an air-cooled finned-tube heat exchanger for precooling the sodium stream and an EM flowmeter for detecting the change in sodium flow rate at plugging temperature. The secondary-loop system does not have its own pump. Sodium flow through the secondary loop is established by the pressure differential in the primary sodium loop across the points of connection of the two loops. Valves are provided in the secondary loop so that, in addition to measuring the plugging temperature of the sodium in the main loop, it is possible to test the quality of the sodium passing through the cold trap.

The entire loop system and tanks (except for the heat exchanger) are traced with heaters and covered with pipe insulation. The individual tubes in the heat exchanger are not traced with heaters. Resistance heater elements are installed in the air duct in the exchanger, and the entire air plenum is covered with block insulation to permit preheating the heat exchanger as a unit.

Extensive control panels are provided for automatic and manual control of the loop operation (see Fig. B.3).

Fig. B.3. Partial View of Control Panels on Operating Floor of Sodium Loop. ANL Neg. No. 900-1929.

APPENDIX C

Method of Calculation of Heat Transfer Coefficient, h*

Figure C.1 is a schematic representation of the temperature profiles in the heater sheath and subchannel coolant before and during gas-jet impingement. The heat-transfer coefficient in the impingement area is defined as follows:

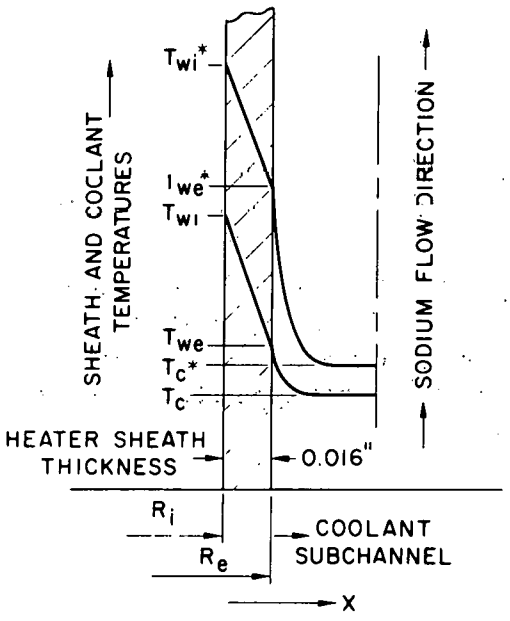

Fig. C.1. Schematic Representation of Temperature Profiles in Heater Sheath and in Subchannel Coolant, before and during Gas-jet Impingement. ANL Neg. No. 900-1332.

$$h^* = \frac{(q'')^*}{T^*_{we} - T^*_c}. \tag{C.1}$$

From Fig. C.1, one finds

$$T^*_{wi} - T^*_c = (T^*_{wi} - T^*_{we}) + (T^*_{we} - T^*_c) \tag{C.2}$$

and

$$T_{wi} - T_c = (T_{wi} - T_{we}) + (T_{we} - T_c). \tag{C.3}$$

Subtracting Eq. C.3 from Eq. C.2 and rearranging results in

$$T^*_{we} - T^*_c = (T^*_{wi} - T_{wi}) - (T^*_c - T_c) + (T_{we} - T_c) + (T_{wi} - T_{we}) - (T^*_{wi} - T^*_{we}). \tag{C.4}$$

The temperature drop in the heater sheath is found from

$$T_{wi} - T_{we} = \frac{q'' R_e \ln (R_e/R_i)}{k_p}. \tag{C.5}$$

If $q'' = (q'')^*$, i.e., the electric power to the heaters remains constant, and the axial and circumferential heat conduction in the pin sheath out of the affected area into the surrounding cooler areas is neglected, one finds

$$T_{wi} - T_{we} = T^*_{wi} - T^*_{we}. \tag{C.6}$$

Substituting Eqs. C.4 and C.6 into Eq. C.1 yields

$$h^* = \frac{q''}{(T^*_{wi} - T_{wi}) - (T^*_c - T_c) + (T_{we} - T_c)}, \tag{C.7}$$

where $T^*_{wi} - T_{wi}$ represents the change in the internal sheath-wall temperature, as measured by the internal thermocouples; $T^*_c - T_c$ represents the

change in the local coolant bulk temperature of the central subchannel, which is equal to zero if coolant flow and power are maintained constant; $T_{we} - T_c$ represents the temperature difference between the external sheath wall and the subchannel coolant bulk temperature prior to gas release, which is calculated from

$$T_{we} - T_c = \frac{q''}{h}, \tag{C.8}$$

where h is found from

$$Nu = \frac{hD_e}{k} = 7.0 + 0.025Re^{0.8}Pr^{0.8}. \tag{C.9}$$

Substitution of $T^*_{wi} - T_{wi}$ (as measured), $T^*_c - T_c$ (as measured and corrected for flow and power variations), and $T_{we} - T_c$ (as calculated) into Eq. C.7 then yields the local value of h* for the particular operating conditions under consideration. The last column of the table in Appendix D gives these calculated values for h* for each test run.

APPENDIX D

Operating Conditions for Individual Test Runs*

*The column headings used in this appendix are computer symbols listed in the Nomenclature.

TEST NO.	GAS	NID	Q*	MF	TI	PI	PS	PE	Z	MF*	TG*	PG*	PI*	PS*	PE*	PG*/PS*	DT*	H*
33 3 2046	AR	.058	123	687	318	4.0	3.7	2.5	.00	600	510	12.9	4.1	3.9	2.5	3.3	32	4.2
33 3 2644	AR	.058	125	690	318	4.1	3.8	2.5	.00	693	510	14.0	4.6	4.3	2.5	3.2	37	2.8
33 3 3246	AR	.058	124	704	320	4.1	3.8	2.5	.00	690	510	14.0	4.5	4.3	2.6	3.3	37	3.0
33 3 3844	AR	.058	123	694	320	4.1	3.8	2.6	.00	695	510	27.8	4.9	4.7	2.6	5.9	24	4.4
33 3 6244	AR	.058	126	688	318	4.1	3.9	2.6	.00	681	510	27.8	4.9	4.7	2.6	5.9	31	3.5
33 3 8038	AR	.058	128	675	311	4.1	3.8	2.5	.00	683	510	41.1	5.2	5.0	2.6	8.3	26	4.3
35 2 696	AR	.058	127	691	327	4.1	3.8	2.6	.00	691	510	6.3	4.1	3.9	2.5	1.6	93	1.3
35 2 1290	AR	.058	127	690	328	4.1	3.8	2.6	.00	692	510	7.9	4.1	3.9	2.4	2.0	90	1.3
35 2 1890	AR	.058	126	689	328	4.1	3.8	2.6	.00	698	510	7.9	3.9	3.7	2.1	2.2	94	1.2
35 2 2490	AR	.058	128	692	329	4.1	3.8	2.6	.00	691	510	21.3	4.0	3.8	1.7	5.6	27	3.9
35 8 406	AR	.058	126	689	328	4.1	3.9	2.8	.00	687	510	54.4	4.7	4.5	1.5	12.1	21	5.1
3510 402	AR	.058	126	691	328	4.1	3.9	2.8	.00	690	510	54.5	4.8	4.6	1.5	12.0	21	5.1
3513 766	AR	.058	127	686	326	4.0	3.8	2.7	.00	676	510	41.1	4.3	4.1	1.4	10.0	21	4.9
3515 454	AR	.058	128	690	328	4.1	3.9	2.8	.00	681	510	35.5	4.1	3.9	1.4	9.0	23	4.6
36 2 464	AR	.058	127	689	322	4.1	3.9	2.8	-.32	683	510	7.4	4.1	3.9	2.5	1.9	22	4.5
36 2 1062	AR	.058	125	681	321	4.1	3.9	2.8	-.32	694	510	7.4	4.1	3.9	2.5	1.9	17	4.8
36 2 1661	AR	.058	126	689	320	4.1	3.9	2.8	-.32	688	510	14.5	4.1	4.0	2.3	3.7	7	9.5
36 2 2261	AR	.058	125	695	320	4.1	3.9	2.8	-.32	697	510	14.5	4.1	3.9	2.3	3.7	8	9.1
36 2 2860	AR	.058	124	690	320	4.1	3.9	2.8	-.32	681	510	28.0	4.1	3.9	1.8	7.1	4	13.3
36 4 470	AR	.058	126	680	315	4.1	3.9	2.8	-.32	684	510	28.1	4.1	3.9	1.8	7.2	8	10.3
36 6 471	AR	.058	126	682	322	4.1	3.9	2.8	-.32	679	510	40.6	4.1	4.0	1.4	10.2	6	11.0
36 8 473	AR	.058	128	685	316	4.1	3.9	2.9	-.32	685	510	41.6	4.2	4.0	1.4	10.4	8	10.1
3610 467	AR	.058	127	687	314	4.1	3.9	2.8	-.32	692	510	54.8	4.6	4.4	1.5	12.4	10	8.6
3612 463	AR	.058	125	676	317	4.1	3.9	2.8	-.32	678	510	54.9	4.6	4.4	1.5	12.5	9	9.4
3614 390	AR	.058	127	687	309	4.1	3.9	2.8	-.32	685	510	47.8	4.4	4.2	1.4	11.4	11	8.6
3617 365	AR	.058	124	690	312	4.1	3.9	2.8	-.32	682	510	47.8	4.4	4.2	1.4	11.4	10	9.3
3620 545	AR	.058	127	686	318	4.1	3.9	2.9	-.32	678	510	34.7	4.1	3.9	1.5	8.9	7	10.1
3622 463	AR	.058	128	693	318	4.1	3.9	2.9	-.32	687	510	34.7	4.1	3.9	1.4	9.0	8	10.6
3624 484	AR	.058	126	694	319	4.1	3.9	2.9	-.32	686	510	20.8	4.2	4.0	2.2	5.2	11	7.9
3626 526	AR	.058	126	687	320	4.1	3.9	2.8	-.32	683	510	20.8	4.1	3.9	2.1	5.4	10	8.9
37 2 412	AR	.058	126	686	322	4.1	4.0	3.5	-.16	685	510	7.0	4.1	4.0	3.1	1.8	90	1.3
37 2 1004	AR	.058	126	685	319	4.1	4.0	3.6	-.16	689	510	7.0	4.1	4.0	3.1	1.8	72	1.6
37 2 1604	AR	.058	127	695	318	4.1	4.0	3.6	-.16	690	510	14.2	4.1	4.0	2.7	3.5	32	3.4
37 2 2203	AR	.058	128	687	318	4.1	4.0	3.5	-.16	691	510	14.2	4.1	4.0	2.7	3.6	32	3.3
37 2 2803	AR	.058	126	698	319	4.1	4.0	3.5	-.16	694	510	27.4	4.1	4.0	2.0	6.8	25	4.1
37 4 473	AR	.058	126	691	312	4.1	4.0	3.5	-.16	688	510	28.3	4.1	4.0	2.0	7.1	32	3.5
37 6 479	AR	.058	126	674	316	4.1	4.0	3.5	-.16	684	510	41.0	4.2	4.2	1.5	9.9	39	2.8
37 2 487	AR	.058	124	684	316	4.1	4.0	3.6	-.16	680	510	41.0	4.2	4.2	1.5	9.8	25	4.3
37 4 434	AR	.058	127	690	318	4.1	4.0	3.5	-.16	690	510	54.5	4.7	4.6	1.6	11.9	27	3.9
37 2 512	AR	.058	127	683	311	4.1	4.0	3.5	-.16	671	510	54.4	4.5	4.4	1.7	12.3	34	3.4
37 4 374	AR	.058	125	686	307	4.1	4.0	3.5	-.16	675	510	48.7	4.4	4.3	1.6	11.3	33	3.5
37 6 491	AR	.058	125	685	317	4.1	4.0	3.6	-.16	680	510	48.8	4.4	4.3	1.6	11.3	32	3.5

ANL Neg. No. 900-2570

TEST NO.	GAS	NID	Q*	MF	TI	PI	PS	PE	Z	MF*	TG*	PG*	PI*	PS*	PE*	PG*/PS*	DT*	H*
37 8 508	AR	.058	126	685	315	4.1	4.0	3.5	-.16	678	510	35.4	4.1	4.0	1.7	8.9	28	3.8
38 2 454	AR	.058	126	685	322	4.1	4.0	3.6	-.08	684	510	8.0	4.1	4.1	3.2	2.0	103	1.2
38 2 1047	AR	.058	127	680	321	4.1	4.0	3.7	-.08	691	510	8.0	4.1	4.0	3.1	2.0	95	1.2
38 2 1646	AR	.058	127	686	320	4.1	4.0	3.6	-.08	692	510	15.8	4.1	4.0	2.8	3.9	33	3.2
38 2 2246	AR	.058	126	685	320	4.1	4.0	3.6	-.08	692	510	15.0	4.1	4.0	2.6	3.7	35	3.0
38 2 2844	AR	.058	128	698	319	4.1	4.0	3.6	-.08	698	510	27.7	4.1	4.0	2.0	6.9	29	3.7
38 4 528	AR	.058	126	686	307	4.1	4.0	3.5	-.08	698	510	27.8	4.1	4.0	2.1	6.9	29	3.5
38 6 470	AR	.058	126	691	315	4.1	4.0	3.5	-.08	686	510	40.5	4.2	4.1	1.5	9.8	28	4.0
38 8 458	AR	.058	126	693	317	4.1	4.0	3.6	-.08	687	510	40.6	4.2	4.1	1.5	9.9	27	3.9
3810 469	AR	.058	127	690	319	4.1	4.0	3.6	-.08	686	510	55.0	4.6	4.6	1.7	12.1	29	3.7
3812 471	AR	.058	125	685	311	4.1	4.0	3.6	-.08	687	510	55.3	4.6	4.6	1.7	12.1	29	3.7
3814 469	AR	.058	126	687	317	4.1	4.0	3.6	-.08	685	510	47.8	4.4	4.3	1.6	11.1	29	3.8
3816 480	AR	.058	126	689	318	4.1	4.0	3.6	-.08	686	510	47.9	4.4	4.3	1.6	11.1	28	3.7
3818 476	AR	.058	126	687	313	4.1	4.0	3.6	-.08	687	510	34.7	4.1	4.0	1.7	8.7	27	3.8
3820 478	AR	.058	124	679	318	4.0	4.0	3.6	-.08	690	510	34.8	4.1	4.0	1.7	8.6	27	3.8
3822 453	AR	.058	126	693	322	4.1	4.0	3.6	-.08	687	510	21.1	4.1	4.0	2.5	5.3	25	4.1
3824 492	AR	.058	125	684	317	4.1	4.0	3.6	-.08	691	510	21.1	4.1	4.0	2.5	5.3	25	3.9
39 2 530	AR	.058	125	686	320	4.1	4.0	3.6	.08	682	510	6.6	4.0	3.9	3.1	1.7	108	1.1
39 2 1122	AR	.058	125	685	319	4.1	4.0	3.6	.08	697	510	6.6	4.1	4.0	3.1	1.7	102	1.1
39 2 1720	AR	.058	125	695	318	4.1	4.0	3.6	.08	690	510	15.4	4.1	4.0	2.7	3.8	31	3.3
39 2 2318	AR	.058	126	685	318	4.1	4.0	3.5	.08	690	510	15.5	4.1	4.0	2.7	3.9	30	3.4
39 2 2920	AR	.058	125	689	319	4.1	4.0	3.6	.08	688	510	28.3	4.0	3.9	2.0	7.2	26	3.8
39 4 456	AR	.058	126	684	315	4.0	4.0	3.6	.08	686	510	29.2	4.1	4.0	2.0	7.3	27	3.8
39 6 460	AR	.058	125	690	320	4.1	4.0	3.6	.08	687	510	41.5	4.2	4.1	1.6	10.0	24	4.3
39 8 465	AR	.058	125	689	315	4.1	4.0	3.6	.08	690	510	41.5	4.2	4.2	1.6	10.0	24	4.3
3912 446	AR	.058	127	690	309	4.1	4.0	3.6	.08	687	510	54.6	4.6	4.5	1.7	12.9	27	4.1
3914 476	AR	.058	126	686	319	4.1	4.0	3.6	.08	689	510	54.6	4.6	4.6	1.7	12.0	26	4.1
3916 484	AR	.058	127	686	322	4.1	4.0	3.6	.08	679	510	48.4	4.4	4.3	1.6	11.2	25	4.1
3918 477	AR	.058	128	691	316	4.1	4.0	3.6	.08	694	510	34.9	4.1	4.0	1.6	8.7	26	4.0
3920 468	AR	.058	126	688	323	4.1	4.0	3.6	.08	685	510	21.1	4.0	4.0	2.5	5.3	17	5.6
40 2 539	AR	.058	127	682	321	4.1	4.0	3.6	.16	670	510	7.7	4.1	4.0	3.2	1.9	117	1.0
40 2 1132	AR	.058	126	695	321	4.1	4.0	3.5	.16	689	510	7.7	4.1	4.0	3.1	1.9	115	1.0
40 2 1730	AR	.058	127	691	318	4.1	4.0	3.5	.16	692	510	14.3	4.1	4.0	2.8	3.6	31	3.4
40 2 2330	AR	.058	127	686	319	4.1	4.0	3.5	.16	689	510	14.3	4.0	4.0	2.7	3.6	30	3.3
40 2 2928	AR	.058	126	690	320	4.1	4.0	3.5	.16	697	510	28.0	4.1	4.0	1.9	7.0	27	3.7
40 4 477	AR	.058	126	691	307	4.1	4.0	3.6	.16	686	510	28.1	4.0	4.0	2.0	7.1	30	3.8
40 6 480	AR	.058	126	685	321	4.1	4.0	3.6	.16	685	510	41.6	4.2	4.2	1.6	10.0	23	4.5
40 8 498	AR	.058	127	683	320	4.1	4.0	3.5	.16	679	510	41.7	4.2	4.1	1.6	10.1	23	4.4
4010 504	AR	.058	126	687	324	4.1	4.0	3.5	.16	686	510	55.6	4.7	4.6	1.8	12.1	24	4.1
4012 517	AR	.058	127	692	322	4.1	4.0	3.6	.16	677	510	55.5	4.6	4.6	1.8	12.2	26	4.4
4014 508	AR	.058	126	689	322	4.1	4.0	3.5	.16	683	510	48.5	4.5	4.4	1.7	11.1	24	4.1
4016 491	AR	.058	126	694	322	4.1	4.0	3.6	.16	685	510	48.5	4.5	4.4	1.7	11.1	25	4.3

ANL Neg. No. 900-2566

TEST NO.	GAS	NID	Q*	MF	TI	PI	PS	PE	Z	MF*	TG*	PG*	PI*	PS*	PE*	PG*/PS*	DT*	H*
41 2 486	AR	.058	126	685	321	4.1	4.0	3.6	.32	693	510	7.6	4.1	4.0	3.1	1.9	107	1.1
41 2 1078	AR	.058	126	690	320	4.1	4.0	3.6	.32	690	510	7.6	4.0	4.0	3.1	1.9	104	1.1
41 2 1679	AR	.058	125	700	319	4.1	4.0	3.6	.32	691	510	14.3	4.1	4.0	2.9	3.5	24	4.2
41 2 2279	AR	.058	126	693	320	4.1	4.0	3.6	.32	694	510	14.2	4.1	4.0	2.8	3.6	23	4.1
41 2 2881	AR	.058	126	690	320	4.1	4.0	3.6	.32	691	510	27.7	4.0	4.0	2.0	7.0	24	4.0
41 4 479	AR	.058	127	693	323	4.1	4.0	3.6	.32	693	510	27.7	4.1	4.0	2.1	6.9	25	4.0
41 6 392	AR	.058	126	687	316	4.1	4.0	3.6	.32	684	510	41.6	4.2	4.1	1.6	10.0	22	5.0
41 8 500	AR	.058	127	686	324	4.1	4.0	3.6	.32	686	510	53.2	4.6	4.5	1.8	11.7	21	4.8
42 2 404	AR	.058	125	682	322	3.9	3.8	3.4	.48	692	510	6.9	4.0	3.9	3.1	1.8	84	1.4
42 2 994	AR	.058	126	697	320	4.0	3.9	3.6	.48	702	510	8.0	4.0	3.9	3.1	2.0	91	1.3
42 2 1594	AR	.058	126	691	319	4.0	3.9	3.6	.48	693	510	14.8	4.0	4.0	2.8	3.7	22	4.6
42 2 2192	AR	.058	126	672	319	3.9	3.9	3.6	.48	696	510	14.8	4.1	4.0	2.9	3.7	20	4.3
42 2 2792	AR	.058	126	683	318	4.1	4.0	3.7	.48	694	510	27.4	4.0	4.0	2.1	6.9	22	4.4
42 4 506	AR	.058	125	689	322	4.1	4.1	3.7	.48	687	510	27.5	4.1	4.0	2.2	6.9	21	4.6
42 6 512	AR	.058	126	694	321	4.1	4.0	3.6	.48	688	510	41.5	4.2	4.2	1.7	10.0	17	5.8
42 8 504	AR	.058	126	694	321	4.1	4.0	3.6	.48	685	510	41.6	4.2	4.2	1.7	10.0	18	5.9
4210 508	AR	.058	124	688	322	4.0	4.0	3.6	.48	679	510	55.1	4.6	4.6	1.9	12.1	18	5.4
4212 504	AR	.058	126	687	321	4.0	4.0	3.6	.48	688	510	55.3	4.6	4.6	1.9	12.0	20	5.5
4214 488	AR	.058	126	690	318	4.1	4.0	3.6	.48	689	510	48.9	4.5	4.4	1.8	11.1	18	5.8
4216 498	AR	.058	127	692	321	4.1	4.0	3.7	.48	688	510	49.0	4.5	4.4	1.8	11.2	18	5.4
4218 496	AR	.058	126	694	319	4.1	4.0	3.7	.48	678	510	35.9	4.1	4.0	1.7	9.0	16	5.8
4220 496	AR	.058	127	687	325	4.1	4.0	3.7	.48	681	510	36.0	4.0	4.0	1.6	9.0	17	5.8
4222 408	AR	.058	126	685	318	4.1	4.0	3.7	.48	683	510	21.9	4.1	4.0	2.5	5.5	23	4.3
4224 514	AR	.058	127	691	318	4.1	4.0	3.6	.48	688	510	21.9	4.1	4.1	2.6	5.4	19	5.4
43 2 520	AR	.058	126	682	324	4.1	4.0	3.7	.63	688	510	7.1	4.1	4.1	3.3	1.7	50	2.2
43 2 1112	AR	.058	127	691	321	4.1	4.0	3.6	.63	691	510	7.1	4.1	4.1	3.3	1.7	43	2.6
43 2 1712	AR	.058	126	689	320	4.1	4.0	3.7	.63	693	510	14.5	4.0	3.9	2.7	3.7	18	5.0
43 2 2312	AR	.058	125	684	320	4.1	4.0	3.7	.63	692	510	14.5	4.2	4.1	3.0	3.5	16	5.4
43 2 2914	AR	.058	127	691	321	4.1	4.0	3.7	.63	691	510	28.8	4.1	4.0	2.1	7.1	15	5.8
43 4 516	AR	.058	125	692	322	4.1	4.0	3.6	.63	684	510	28.8	4.1	4.0	2.1	7.2	16	6.0
43 6 490	AR	.058	126	696	315	4.1	4.0	3.6	.63	692	510	41.0	4.2	4.2	1.7	9.8	16	5.8
43 8 496	AR	.058	126	693	322	4.1	4.0	3.7	.63	695	510	41.6	4.3	4.2	1.7	9.9	15	6.1
4310 514	AR	.058	127	682	322	4.1	4.0	3.7	.63	688	510	54.3	4.6	4.6	1.9	11.9	16	5.3
4312 518	AR	.058	126	690	320	4.1	4.0	3.6	.63	684	510	54.4	4.6	4.6	1.9	11.9	19	5.2
4314 516	AR	.058	127	691	321	4.1	4.0	3.7	.63	693	510	48.9	4.5	4.4	1.8	11.0	18	5.0
4316 520	AR	.058	125	681	321	4.0	4.0	3.7	.63	689	510	49.0	4.4	4.4	1.7	11.2	18	5.0
4318 506	AR	.058	128	688	323	4.1	4.0	3.6	.63	687	510	35.3	4.1	4.0	1.7	8.7	15	6.1
4320 512	AR	.058	127	691	314	4.1	4.0	3.6	.63	688	510	35.3	4.1	4.0	1.6	8.9	17	5.7
4322 516	AR	.058	128	685	318	4.1	4.0	3.7	.63	689	510	20.4	4.1	4.0	2.6	5.1	21	4.9
4324 424	AR	.058	127	692	317	4.1	4.0	3.6	.63	686	510	21.5	4.1	4.0	2.5	5.4	20	5.0
44 2 440	AR	.058	126	696	321	4.1	4.1	3.7	.95	692	510	8.1	4.1	4.1	3.3	2.0	17	5.7
44 2 1042	AR	.058	126	680	318	4.1	4.0	3.7	.95	691	510	8.1	4.1	4.0	3.2	2.0	16	5.2

ANL Neg. No. 900-2571

TEST NO.	GAS	NID	Q*	MF	TI	PI	PS	PE	Z	MF*	TG*	PG*	PI*	PS*	PE*	PG*/PS*	DT*	H*
44 2 1638	AR	.058	124	692	318	4.1	4.0	3.6	.95	691	510	14.3	4.1	4.1	2.9	3.5	11	7.2
44 2 2238	AR	.058	126	686	317	4.1	4.0	3.7	.95	692	510	14.3	4.1	4.0	2.8	3.6	11	6.7
44 2 2836	AR	.058	125	678	318	4.1	4.0	3.7	.95	688	510	27.5	4.0	3.9	2.1	7.0	11	6.5
44 4 384	AR	.058	125	689	317	4.1	4.0	3.6	.95	684	510	27.5	4.1	4.0	2.3	6.8	10	9.5
44 6 518	AR	.058	127	701	321	4.1	4.0	3.6	.95	691	510	40.6	4.1	4.1	1.6	10.0	15	6.4
44 8 518	AR	.058	126	694	319	4.1	4.0	3.7	.95	695	510	40.6	4.1	4.1	1.5	10.0	16	5.9
4410 516	AR	.058	127	701	328	4.1	4.0	3.6	.95	687	510	54.9	4.5	4.5	1.8	12.3	16	6.0
45 2 376	AR	.058	128	690	322	4.1	4.0	3.6	.95	694	510	7.8	4.0	4.0	3.1	2.0	17	5.0
45 2 976	AR	.058	127	694	321	4.1	4.0	3.6	.95	687	510	7.8	4.1	4.0	3.2	1.9	15	6.0
45 2 1576	AR	.058	126	689	318	4.1	4.0	3.6	.95	689	510	14.5	4.1	4.0	2.9	3.6	13	6.7
45 2 2176	AR	.058	128	689	320	4.1	4.0	3.6	.95	687	510	14.5	4.1	4.0	2.9	3.6	13	6.3
45 2 2776	AR	.058	128	685	318	4.1	4.0	3.7	.95	694	510	28.1	4.1	4.1	2.1	6.9	12	6.9
45 4 506	AR	.058	127	685	318	4.1	4.0	3.7	.95	694	510	28.1	4.1	4.0	2.1	7.0	13	6.6
45 6 510	AR	.058	126	685	314	4.1	4.0	3.7	.95	685	510	41.3	4.2	4.2	1.6	9.9	16	5.4
45 8 522	AR	.058	126	689	314	4.1	4.1	3.7	.95	690	510	41.3	4.2	4.2	1.6	9.9	15	5.7
4510 510	AR	.058	128	680	325	4.1	4.0	3.7	.95	695	510	55.1	4.7	4.6	1.8	11.9	16	5.9
4512 504	AR	.058	127	683	321	4.1	4.0	3.7	.95	688	510	55.2	4.6	4.6	1.8	12.1	16	6.0
4514 526	AR	.058	126	689	314	4.1	4.0	3.7	.95	683	510	48.8	4.4	4.4	1.7	11.1	17	5.8
4516 506	AR	.058	126	689	317	4.0	4.0	3.6	.95	685	510	48.7	4.4	4.4	1.7	11.2	17	5.8
4518 522	AR	.058	126	696	320	4.1	4.0	3.6	.95	691	510	35.0	4.1	4.0	1.6	8.8	13	6.4
4520 522	AR	.058	126	681	312	4.1	4.0	3.7	.95	690	510	35.0	4.1	4.0	1.7	8.7	13	6.2
4522 520	AR	.058	127	689	318	4.1	4.1	3.7	.95	687	510	21.4	4.0	3.9	2.4	5.4	18	5.3
4524 518	AR	.058	127	690	315	4.1	4.0	3.6	.95	687	510	21.4	4.1	4.1	2.6	5.3	17	5.4
46 2 474	AR	.058	127	683	325	4.1	4.0	3.7	1.11	690	510	7.6	4.1	4.0	3.2	1.9	13	6.7
46 2 1074	AR	.058	125	679	324	4.1	4.0	3.7	1.11	690	510	7.5	3.9	3.9	3.0	1.9	13	6.2
46 2 1676	AR	.058	126	697	324	4.1	4.0	3.7	1.11	693	510	14.3	4.2	4.1	3.0	3.5	11	6.7
46 2 2276	AR	.058	127	697	321	4.1	4.0	3.7	1.11	689	510	14.3	4.1	4.0	2.9	3.5	12	7.9
46 2 2876	AR	.058	127	686	323	4.1	4.0	3.7	1.11	691	510	14.3	4.0	3.9	2.7	3.7	13	6.2
46 2 3476	AR	.058	126	686	322	4.1	4.0	3.7	1.11	691	510	28.2	4.0	4.0	2.1	7.1	9	8.1
46 4 320	AR	.058	126	681	316	4.1	4.1	3.7	1.11	687	510	28.3	4.0	3.9	1.9	7.2	6	10.2
46 6 506	AR	.058	126	689	311	4.1	4.0	3.7	1.11	679	510	41.6	4.2	4.1	1.6	10.2	16	6.1
46 8 302	AR	.058	127	682	317	4.1	4.0	3.7	1.11	689	510	41.6	4.2	4.1	1.6	10.0	15	5.6
4610 518	AR	.058	125	693	316	4.1	4.0	3.6	1.11	689	510	56.0	4.6	4.6	1.8	12.3	14	6.4
4613 490	AR	.058	128	690	319	4.1	4.0	3.7	1.11	686	510	56.0	4.6	4.6	1.8	12.3	15	6.7
4615 526	AR	.058	125	689	315	4.1	4.0	3.6	1.11	684	510	48.8	4.4	4.3	1.7	11.2	15	6.2
4617 514	AR	.058	127	685	319	4.1	4.0	3.7	1.11	681	510	48.8	4.4	4.3	1.7	11.2	15	6.2
4619 520	AR	.058	126	689	320	4.1	4.0	3.7	1.11	677	510	35.0	4.1	4.0	1.8	8.7	14	6.0
4621 520	AR	.058	126	689	312	4.1	4.0	3.6	1.11	683	510	35.0	4.0	3.9	1.7	8.9	16	6.2
4623 522	AR	.058	127	692	311	4.1	4.0	3.6	1.11	686	510	21.0	4.1	4.1	2.6	5.2	15	6.4
4625 526	AR	.058	127	690	320	4.1	4.0	3.6	1.11	690	510	21.1	4.1	4.1	2.6	5.2	14	5.9
47 2 372	AR	.058	126	680	335	4.1	4.0	3.8	1.27	686	510	6.9	4.1	4.1	3.4	1.7	10	7.5
47 2 972	AR	.058	126	689	341	4.1	4.1	3.8	1.27	693	510	8.1	4.1	4.0	3.3	2.0	12	6.3

ANL Neg. No. 900-2572

TEST NO.	GAS	NID	Q*	MF	TI	PI	PS	PE	Z	MF*	TG*	PG*	PI*	PS*	PE*	PG*/PS*	DT*	H*
47 2 1570	AR	.058	126	696	334	4.1	4.0	3.8	1.27	699	510	14.6	4.1	4.1	3.1	3.6	9	6.4
47 2 2170	AR	.058	125	689	323	4.1	4.0	3.8	1.27	688	510	14.6	4.1	4.0	3.0	3.6	15	5.6
47 2 2770	AR	.058	125	689	315	4.1	4.0	3.8	1.27	697	510	28.1	4.1	4.1	2.3	6.9	9	8.1
47 4 518	AR	.058	125	688	310	4.1	4.1	3.8	1.27	683	510	28.2	4.0	4.0	2.2	7.1	13	8.4
47 6 520	AR	.058	126	693	314	4.1	4.0	3.7	1.27	687	510	40.5	4.2	4.1	1.7	9.9	13	7.1
47 8 520	AR	.058	126	688	319	4.1	4.0	3.7	1.27	682	510	41.5	4.2	4.1	1.7	10.1	13	7.5
4710 514	AR	.058	126	687	311	4.1	4.0	3.7	1.27	693	510	55.6	4.6	4.6	1.9	12.2	11	6.6
4712 506	AR	.058	126	687	309	4.1	4.1	3.8	1.27	683	510	55.7	4.6	4.5	1.9	12.4	11	7.6
4714 514	AR	.058	125	692	315	4.1	4.0	3.8	1.27	686	510	48.7	4.4	4.3	1.8	11.3	13	7.
4716 508	AR	.058	127	695	315	4.1	4.0	3.8	1.27	689	510	48.7	4.4	4.3	1.8	11.3	13	6.2
4718 508	AR	.058	126	688	315	4.1	4.1	3.8	1.27	689	510	35.3	4.1	4.1	2.0	8.7	15	7.1
4720 514	AR	.058	125	691	313	4.1	4.1	3.8	1.27	690	510	35.3	4.1	4.0	1.9	8.7	15	7.3
4722 514	AR	.058	126	686	320	4.1	4.0	3.8	1.27	689	510	21.3	4.1	4.1	2.7	5.3	14	5.7
4724 508	AR	.058	126	693	313	4.1	4.1	3.8	1.27	689	510	21.3	4.1	4.1	2.7	5.2	12	7.7
48 2 464	AR	.058	126	683	322	4.1	4.0	3.8	.95	684	510	8.1	4.1	4.0	3.3	2.0	15	5.6
48 2 1058	AR	.058	127	689	317	4.0	4.0	3.7	.95	688	510	8.1	4.1	4.1	3.4	2.0	20	4.9
48 2 1660	AR	.058	126	691	318	4.1	4.1	3.8	.95	691	510	14.8	4.1	4.1	3.0	3.6	11	7.0
48 2 2260	AR	.058	126	687	315	4.1	4.0	3.7	.95	693	510	14.8	4.1	4.0	3.0	3.7	11	6.7
48 2 2860	AR	.058	126	687	315	4.1	4.1	3.7	.95	691	510	28.3	4.1	4.0	2.3	7.0	14	6.2
48 4 524	AR	.058	126	695	310	4.1	4.0	3.7	.95	691	510	28.3	4.1	4.1	2.4	7.0	12	7.8
48 6 1116	AR	.058	127	692	317	4.1	4.0	3.7	.95	693	510	41.7	4.2	4.1	1.7	10.2	17	5.2
48 8 526	AR	.058	126	690	306	4.1	4.0	3.7	.95	692	510	41.8	4.1	4.1	1.7	10.2	17	5.6
4810 522	AR	.058	126	692	313	4.1	4.0	3.7	.95	694	510	55.4	4.5	4.5	1.8	12.3	20	4.9
4812 520	AR	.058	125	691	311	4.1	4.0	3.8	.95	695	510	55.5	4.5	4.5	1.8	12.4	19	5.5
4814 522	AR	.058	127	694	309	4.1	4.0	3.7	.95	693	510	48.5	4.3	4.3	1.7	11.4	18	4.6
4816 523	AR	.058	126	691	314	4.1	4.0	3.7	.95	690	510	48.6	4.3	4.3	1.7	11.4	17	6.0
4818 517	AR	.058	126	694	313	4.1	4.0	3.7	.95	699	510	35.3	4.2	4.1	2.0	8.6	14	5.3
4820 528	AR	.058	126	691	314	4.1	4.0	3.7	.95	695	510	35.3	4.1	4.1	2.0	8.7	15	6.9
4822 515	AR	.058	127	691	313	4.1	4.0	3.7	.95	694	510	21.1	4.1	4.1	2.7	5.2	22	4.7
4824 526	AR	.058	126	696	313	4.1	4.0	3.7	.95	692	510	21.1	4.3	4.2	3.0	5.0	20	5.1
49 2 496	AR	.058	126	696	319	4.1	4.0	3.7	.00	693	510	5.2	4.0	4.0	3.4	1.3	22	4.5
49 2 1086	AR	.058	126	690	317	4.1	4.0	3.7	.00	692	510	5.2	4.1	4.0	3.5	1.3	32	3.3
49 2 1686	AR	.058	126	691	317	4.1	4.0	3.7	.00	696	510	6.5	4.1	4.0	3.4	1.6	96	1.2
49 2 2286	AR	.058	125	690	317	4.1	4.0	3.8	.00	693	510	6.4	4.1	4.0	3.4	1.6	99	1.2
49 2 2888	AR	.058	125	691	318	4.1	4.0	3.7	.00	691	510	7.3	4.1	4.0	3.4	1.8	101	1.2
49 2 3490	AR	.058	126	694	317	4.1	4.0	3.7	.00	693	510	7.3	4.1	4.0	3.3	1.8	104	1.2
49 2 4091	AR	.058	126	693	316	4.1	4.0	3.7	.00	697	510	7.9	4.1	4.0	3.3	2.0	109	1.1
49 2 4691	AR	.058	125	686	317	4.1	4.0	3.8	.00	690	510	7.9	4.1	4.0	3.3	2.0	111	1.1
49 2 5291	AR	.058	125	695	318	4.1	4.0	3.7	.00	696	510	8.6	4.1	4.0	3.2	2.1	107	1.1
49 2 5891	AR	.058	126	690	318	4.1	4.0	3.7	.00	693	510	8.6	4.1	4.0	3.2	2.1	109	1.1
49 2 6491	AR	.058	125	691	318	4.1	4.1	3.8	.00	689	510	9.3	4.1	4.0	3.2	2.3	108	1.1
49 2 7090	AR	.058	125	690	318	4.1	4.0	3.7	.00	696	510	9.3	4.1	4.0	3.2	2.3	107	1.1

ANL Neg. No. 900-2575

TEST NO.	GAS	NID	Q*	MF	TI	PI	PS	PE	Z	MF*	TG*	PG*	PI*	PS*	PE*	PG*/PS*	DT*	H*
49 2 7691	AR	.058	125	689	318	4.1	4.0	3.8	.00	692	510	10.2	4.1	4.0	3.2	2.5	108	1.1
49 2 8291	AR	.058	125	689	318	4.1	4.0	3.7	.00	693	510	10.2	4.1	4.0	3.2	2.5	95	1.2
49 2 8893	AR	.058	125	700	317	4.1	4.0	3.7	.00	697	510	48.7	4.4	4.3	1.8	11.2	31	3.4
49 4 519	AR	.058	127	694	309	4.1	4.0	3.7	.00	689	510	48.8	4.4	4.3	1.8	11.3	32	3.4
50 2 3386	AR	.058	26	144	313	2.0	2.0	2.0	.00	150	510	6.4	2.1	2.1	2.0	3.1	2	4.7
50 2 3985	AR	.058	26	150	315	2.1	2.1	2.0	.00	143	510	7.6	2.1	2.1	2.0	3.7	4	6.8
50 2 4587	AR	.058	27	145	310	2.1	2.0	2.0	.00	147	510	14.1	2.1	2.1	1.9	6.9	5	3.6
50 2 5187	AR	.058	27	147	307	2.1	2.0	2.0	.00	151	510	14.1	2.0	2.0	1.9	6.9	4	3.4
50 2 6388	AR	.058	27	146	311	2.1	2.1	2.1	.00	149	510	20.9	2.1	2.1	1.9	10.0	8	2.4
50 2 6988	AR	.058	27	147	312	2.0	2.0	2.0	.00	152	510	27.7	2.1	2.1	1.8	13.5	9	2.7
50 4 507	AR	.058	26	143	308	2.1	2.1	2.0	.00	150	510	27.7	2.1	2.1	1.8	13.4	9	2.2
50 6 518	AR	.058	25	145	315	2.0	2.0	2.0	.00	146	510	34.8	2.0	2.0	1.7	17.2	11	2.1
50 8 514	AR	.058	27	144	309	2.1	2.1	2.0	.00	152	510	34.7	2.1	2.1	1.8	16.5	11	1.8
5010 521	AR	.058	26	145	314	2.1	2.0	2.0	.00	149	510	41.5	2.1	2.1	1.8	19.9	12	1.7
5012 528	AR	.058	25	145	313	2.0	2.0	2.0	.00	157	510	41.3	2.1	2.1	1.7	20.0	11	1.8
51 2 1042	AR	.058	27	146	322	2.0	2.0	2.0	.00	145	510	7.7	2.1	2.1	2.0	3.7	3	5.9
51 2 1644	AR	.058	27	146	321	2.0	2.0	2.0	.00	146	510	4.0	2.1	2.0	2.0	2.0	2	4.8
51 2 2244	AR	.058	26	150	320	2.0	2.0	2.0	.00	148	510	4.0	2.1	2.1	2.0	1.9	2	14.6
51 2 2847	AR	.058	26	150	318	2.0	2.0	2.0	.00	149	510	5.7	2.1	2.1	2.0	2.8	2	10.0
51 2 3447	AR	.058	27	149	318	2.0	2.0	2.0	.00	149	510	5.7	2.1	2.1	2.0	2.8	2	4.2
51 2 4049	AR	.058	27	144	317	2.0	2.0	2.0	.00	152	510	9.3	2.1	2.0	1.9	4.5	4	2.1
51 2 4651	AR	.058	27	145	316	2.0	2.0	2.0	.00	146	510	9.3	2.1	2.1	2.0	4.5	4	6.1
51 2 5252	AR	.058	27	146	314	2.0	2.0	2.0	.00	148	510	10.9	2.1	2.1	2.0	5.3	5	2.8
51 2 5852	AR	.058	27	148	313	2.0	2.0	2.0	.00	147	510	10.9	2.1	2.1	2.0	5.3	4	5.1
51 4 452	AR	.058	26	148	303	2.1	2.1	2.0	.00	145	510	48.5	2.1	2.1	1.7	23.6	14	1.9
51 6 496	AR	.058	26	149	323	2.0	2.0	2.0	.00	144	510	48.7	2.1	2.1	1.7	23.6	13	1.9
51 8 500	AR	.058	26	149	308	2.0	2.0	2.0	.00	146	510	54.9	2.0	2.0	1.6	27.2	13	2.0
5110 511	AR	.058	27	147	309	2.0	2.0	2.0	.00	141	510	55.1	2.0	2.0	1.6	27.2	15	1.5
52 2 509	AR	.058	125	684	320	4.1	3.9	3.0	.00	689	720	14.4	4.1	3.9	2.3	3.7	18	5.3
52 2 1109	AR	.058	125	685	319	4.1	3.9	3.0	.00	696	720	14.4	4.1	4.0	2.4	3.6	18	5.0
52 2 1709	AR	.058	126	698	318	4.1	3.9	2.9	.00	696	720	12.6	4.1	3.9	2.4	3.2	37	2.9
52 2 2308	AR	.058	125	693	319	4.1	3.9	2.9	.00	687	720	12.6	4.1	3.9	2.4	3.2	36	3.0
52 2 2908	AR	.058	126	693	318	4.1	3.9	2.9	.00	695	720	10.8	4.1	3.9	2.4	2.8	43	2.5
52 2 3507	AR	.058	126	687	318	4.1	3.9	2.9	.00	691	720	10.8	4.1	3.9	2.5	2.8	43	2.5
52 2 4107	AR	.058	126	691	318	4.1	3.9	3.0	.00	694	720	9.0	4.1	3.9	2.5	2.3	108	1.1
52 2 4707	AR	.058	124	697	318	4.1	3.9	2.9	.00	693	720	9.0	4.1	3.9	2.5	2.3	108	1.1
52 3 452	AR	.058	125	693	319	4.1	3.9	2.9	.00	696	720	7.1	4.1	3.9	2.6	1.8	112	1.1
52 3 1051	AR	.058	125	689	318	4.1	3.9	2.9	.00	691	720	7.1	4.1	3.9	2.6	1.8	113	1.0
52 3 1651	AR	.058	127	688	318	4.1	3.9	2.9	.00	686	720	5.5	4.1	3.9	2.7	1.4	96	1.3
52 3 2251	AR	.058	127	687	319	4.1	3.9	3.0	.00	695	720	5.5	4.1	3.9	2.7	1.4	94	1.3
52 3 2850	AR	.058	127	689	318	4.1	3.9	2.9	.00	696	720	21.2	4.1	3.9	2.1	5.4	26	3.7
52 5 534	AR	.058	126	685	309	4.1	3.9	3.0	.00	690	720	21.2	4.1	3.9	2.1	5.4	16	5.7

ANL Neg. No. 900-2568

TEST	NC.	GAS	NID	Q*	MF	TI	PI	PS	PE	Z	MF*	TG*	PG*	PI*	PS*	PE*	PG*/PS*	DT*	H*
52 7	474	AR	.058	126	698	325	4.1	3.9	2.9	.00	696	720	28.0	4.1	3.9	1.8	7.2	27	3.7
52 9	486	AR	.058	126	684	319	4.1	3.9	3.0	.00	694	720	28.1	4.1	4.0	1.9	7.1	26	3.8
53 2	484	AR	.058	252	689	325	4.1	3.9	3.0	.00	688	510	13.8	4.1	4.0	2.4	3.5	29	5.9
53 2	1083	AR	.058	252	685	321	4.1	3.9	3.0	.00	693	510	13.7	4.1	3.9	2.4	3.5	62	3.3
53 2	1682	AR	.058	252	691	320	4.1	3.9	3.0	.00	696	510	13.7	4.1	4.0	2.4	3.5	64	3.3
53 2	2282	AR	.058	254	687	321	4.1	3.9	3.0	.00	691	510	12.5	4.1	4.0	2.5	3.1	67	3.1
53 2	2880	AR	.058	252	690	321	4.1	3.9	2.9	.00	685	510	12.4	4.1	4.0	2.5	3.1	67	3.2
53 2	3481	AR	.058	251	682	321	4.1	3.9	3.0	.00	685	510	10.4	4.1	3.9	2.5	2.7	79	2.7
53 2	4080	AR	.058	252	692	320	4.1	3.9	2.9	.00	689	510	10.4	4.1	4.0	2.6	2.6	78	2.8
53 2	4679	AR	.058	252	689	320	4.1	3.9	3.0	.00	684	510	8.7	4.1	3.9	2.6	2.2	144	1.6
53 2	5278	AR	.058	254	691	321	4.1	3.9	3.0	.00	684	510	8.8	4.1	4.0	2.6	2.2	91	2.5
53 2	5878	AR	.058	252	697	320	4.1	3.9	2.9	.00	689	510	7.0	4.1	4.0	2.7	1.8	207	1.2
53 2	6476	AR	.058	252	682	320	4.1	3.9	3.0	.00	690	510	7.0	4.1	3.9	2.6	1.8	206	1.1
53 2	7075	AR	.058	253	693	321	4.1	3.9	2.9	.00	691	510	5.3	4.1	4.0	2.8	1.3	210	1.1
53 2	7674	AR	.058	252	681	320	4.1	3.9	3.0	.00	688	510	5.3	4.1	3.9	2.8	1.4	202	1.2
53 2	8274	AR	.058	252	689	321	4.1	3.9	3.0	.00	690	510	4.9	4.1	4.0	2.9	1.2	67	3.2
53 2	8873	AR	.058	253	686	321	4.1	3.9	3.0	.00	695	510	4.8	4.1	3.9	2.8	1.2	78	2.7
54 2	521	XE	.058	125	678	321	4.1	4.0	3.0	.00	685	510	6.6	4.1	3.9	2.8	1.7	58	1.9
54 2	1112	XE	.058	127	679	318	4.1	3.9	3.0	.00	687	510	20.3	4.1	3.9	2.5	5.1	16	5.3
54 2	1712	XE	.058	125	693	318	4.1	3.9	3.0	.00	689	510	26.6	4.1	3.9	2.4	6.7	14	6.4
54 2	2312	XE	.058	124	682	318	4.1	3.9	3.0	.00	692	510	26.6	4.1	3.9	2.3	6.8	14	5.8
54 2	2913	XE	.058	124	684	318	4.1	4.0	3.0	.00	692	510	14.1	4.1	3.9	2.6	3.6	20	4.5
54 2	3513	XE	.058	126	693	318	4.1	3.9	3.0	.00	690	510	10.0	4.1	3.9	2.7	2.6	43	2.5
54 2	4112	XE	.058	125	689	318	4.1	3.9	3.0	.00	696	510	8.5	4.1	3.9	2.7	2.2	79	1.5
54 2	4712	XE	.058	126	693	318	4.1	3.9	2.9	.00	694	510	8.5	4.1	3.9	2.8	2.2	79	1.5
54 2	5312	XE	.058	126	691	318	4.1	3.9	2.9	.00	697	510	6.7	4.1	3.9	2.8	1.7	75	1.5
54 2	5912	XE	.058	125	693	318	4.1	3.9	3.0	.00	688	510	6.7	4.1	3.9	2.8	1.7	71	1.6
54 2	6511	XE	.058	124	686	318	4.1	3.9	3.0	.00	687	510	5.1	4.1	3.9	2.9	1.3	15	5.9
54 2	7111	XE	.058	125	691	318	4.1	3.9	3.0	.00	687	510	5.9	4.1	3.9	2.8	1.5	51	2.2
54 2	7711	XE	.058	124	689	318	4.1	3.9	2.9	.00	692	510	4.4	4.1	3.9	2.8	1.1	4	12.3
54 2	8311	XE	.058	124	685	318	4.1	3.9	3.0	.00	694	510	4.9	4.1	3.9	2.9	1.2	8	7.9
54 2	8910	XE	.058	125	690	318	4.1	3.9	2.9	.00	690	510	4.8	4.1	3.9	2.9	1.2	8	8.7
54 2	9508	XE	.058	126	687	318	4.1	3.9	3.0	.00	694	510	4.7	4.1	3.9	2.9	1.2	7	9.0
55 2	507	AR	.058	126	695	322	4.1	3.9	2.9	.00	688	510	7.2	4.1	4.0	2.7	1.8	114	1.1
55 2	1107	AR	.058	127	694	320	4.1	3.9	3.0	.00	690	510	7.2	4.1	3.9	2.6	1.9	113	1.1
55 2	1707	AR	.058	128	693	319	4.1	3.9	2.9	.00	690	510	5.3	4.1	3.9	2.8	1.4	51	2.2
55 2	2306	AR	.058	127	680	319	4.1	3.9	3.0	.00	689	510	5.3	4.1	3.9	2.8	1.4	52	2.1
55 2	2906	AR	.058	126	696	319	4.1	3.9	2.9	.00	691	510	8.7	4.1	3.9	2.6	2.2	119	1.0
55 2	3506	AR	.058	127	694	318	4.1	3.9	3.0	.00	689	510	8.7	4.1	3.9	2.6	2.2	120	1.0
55 2	4106	AR	.058	126	685	318	4.1	3.9	3.0	.00	690	510	10.3	4.0	3.9	2.5	2.7	49	2.2
55 2	4707	AR	.058	127	689	318	4.1	3.9	3.0	.00	691	510	10.3	4.1	3.9	2.5	2.6	49	2.3
55 2	5307	AR	.058	127	682	318	4.1	4.0	3.0	.00	690	510	14.0	4.1	3.9	2.4	3.6	34	3.1

ANL Neg. No. 900-2567

TEST NO.	GAS	NID	Q*	MF	TI	PI	PS	PE	Z	MF*	TG*	PG*	PI*	PS*	PE*	PG*/PS*	DT*	H*
55 2 5907	AR	.058	127	687	319	4.1	3.9	3.0	.00	684	510	14.0	4.1	3.9	2.4	3.6	33	3.2
55 2 6507	AR	.058	127	690	318	4.1	3.9	3.0	.00	692	510	27.6	4.1	4.0	1.9	7.0	26	3.8
56 2 458	AR	.084	132	696	332	4.0	3.8	2.9	.00	700	510	6.5	3.9	3.8	2.3	1.7	45	2.5
56 2 1059	AR	.084	131	695	329	3.9	3.8	2.9	.00	707	510	6.7	3.9	3.8	2.3	1.8	51	2.3
56 2 1659	AR	.084	132	700	328	4.0	3.8	2.9	.00	707	510	6.9	3.9	3.8	2.2	1.8	47	2.4
56 2 2260	AR	.084	131	705	327	4.0	3.8	2.9	.00	706	510	6.1	3.9	3.8	2.3	1.6	45	2.5
56 2 2860	AR	.084	131	703	328	3.9	3.8	2.9	.00	697	510	6.2	4.0	3.8	2.4	1.6	43	2.6
56 2 3460	AR	.084	131	698	329	3.9	3.8	2.9	.00	703	510	5.5	4.0	3.8	2.4	1.4	45	2.5
56 2 4060	AR	.084	133	709	331	3.9	3.8	2.9	.00	707	510	5.3	3.9	3.8	2.3	1.4	46	2.5
56 2 4660	AR	.084	132	696	329	3.9	3.8	2.9	.00	705	510	4.6	3.9	3.8	2.4	1.2	69	1.7
56 2 5262	AR	.084	131	698	326	4.0	3.8	2.9	.00	703	510	4.8	3.9	3.8	2.4	1.3	67	1.8
56 2 5862	AR	.084	132	695	328	3.9	3.8	2.9	.00	695	510	4.3	4.0	3.8	2.6	1.1	66	1.8
56 2 6461	AR	.084	131	697	328	3.9	3.8	2.9	.00	691	510	4.3	3.9	3.8	2.5	1.1	68	1.8
56 2 7060	AR	.084	132	702	327	4.0	3.8	2.9	.00	700	510	10.5	4.0	3.8	2.1	2.8	50	2.3
56 4 487	AR	.084	132	700	332	4.0	3.8	2.9	.00	696	510	10.5	4.0	3.8	2.1	2.8	49	2.4
56 6 1095	AR	.084	133	694	330	3.9	3.8	2.9	.00	698	510	13.6	4.0	3.8	1.8	3.6	32	3.4
56 8 481	AR	.084	131	691	331	3.9	3.8	2.9	.00	696	510	13.7	3.9	3.8	1.8	3.6	31	3.5
5610 501	AR	.084	133	699	331	4.0	3.8	2.9	.00	690	510	20.5	4.0	3.9	1.4	5.3	30	3.7
5612 1101	AR	.084	132	694	329	3.9	3.8	2.9	.00	694	510	20.6	4.0	3.9	1.4	5.3	29	3.7
5614 501	AR	.084	133	699	332	3.9	3.8	2.9	.00	694	510	27.6	4.4	4.3	1.6	6.5	35	3.3
5616 119	AR	.084	132	694	331	3.9	3.8	2.9	.00	687	510	27.6	4.4	4.3	1.6	6.5	35	3.3
57 2 484	AR	.084	126	685	318	4.1	3.9	2.9	.00	690	510	7.1	4.1	3.9	2.4	1.8	47	2.3
57 2 1084	AR	.084	125	700	316	4.1	3.9	2.9	.00	693	510	7.1	4.1	4.0	2.4	1.8	45	2.5
57 2 1684	AR	.084	125	692	317	4.1	3.9	2.9	.00	689	510	5.4	4.1	3.9	2.6	1.4	67	1.7
57 2 2283	AR	.084	126	690	317	4.1	3.9	2.9	.00	692	510	5.4	4.1	3.9	2.5	1.4	65	1.7
57 2 2883	AR	.084	126	691	316	4.1	3.9	2.9	.00	696	510	4.8	4.1	3.9	2.6	1.2	27	3.8
57 2 3482	AR	.084	126	689	316	4.1	3.9	2.9	.00	691	510	4.8	4.1	3.9	2.6	1.2	34	3.1
57 2 4082	AR	.084	126	690	318	4.1	3.9	2.9	.00	692	510	9.0	4.1	3.9	2.2	2.3	53	2.1
57 2 4680	AR	.084	125	687	316	4.1	3.9	3.0	.00	692	510	9.0	4.1	3.9	2.2	2.3	51	2.2
57 2 5280	AR	.084	126	687	316	4.1	3.9	3.0	.00	690	510	10.4	4.1	3.9	2.1	2.7	52	2.2
57 4 457	AR	.084	128	685	319	4.1	3.9	2.9	.00	686	510	10.6	4.1	3.9	2.1	2.7	52	2.2
57 6 523	AR	.084	127	687	320	4.1	4.0	3.0	.00	687	510	13.7	4.1	4.0	2.0	3.5	44	2.5
57 8 462	AR	.084	125	691	321	4.1	3.9	2.9	.00	690	510	13.7	4.1	4.0	1.9	3.5	45	2.6
5710 463	AR	.084	127	686	322	4.1	3.9	2.9	.00	679	510	20.6	4.2	4.0	1.4	5.2	28	3.7
5712 475	AR	.084	128	679	320	4.1	3.9	2.9	.00	692	510	20.6	4.2	4.0	1.4	5.1	27	3.6
5714 482	AR	.084	128	685	320	4.1	3.9	3.0	.00	690	510	27.9	4.6	4.5	1.6	6.3	33	3.3
5716 488	AR	.084	126	684	322	4.1	3.9	2.9	.00	684	510	27.9	4.6	4.4	1.6	6.3	34	3.2
5718 477	AR	.084	126	687	319	4.1	3.9	2.9	.00	687	510	24.2	4.4	4.2	1.5	5.7	31	3.5
5720 498	AR	.084	127	687	320	4.1	3.9	2.9	.00	683	510	24.3	4.4	4.2	1.5	5.8	30	3.7
5722 92	AR	.084	128	681	320	4.1	3.9	2.9	.00	679	510	17.5	4.1	3.9	1.5	4.5	27	3.7
5724 79	AR	.084	128	689	319	4.1	3.9	2.9	.00	687	510	17.6	4.1	3.9	1.6	4.5	27	3.7
58 2 508	AR	.033	127	690	321	4.1	3.9	3.0	.00	689	510	7.1	4.1	3.9	2.9	1.8	29	3.6

ANL Neg. No. 900-2565

TEST NO.	GAS	NID	Q*	MF	TI	PI	PS	PE	Z	MF*	TG*	PG*	PI*	PS*	PE*	PG*/PS*	DT*	H*
58 2 1106	AR	.033	127	688	318	4.1	3.9	3.0	.00	693	510	6.7	4.1	3.9	2.9	1.7	29	3.6
58 2 1705	AR	.033	128	700	316	4.1	3.9	2.9	.00	686	510	6.8	4.1	3.9	2.9	1.7	27	3.8
58 2 2303	AR	.033	126	684	318	4.1	4.0	3.0	.00	688	510	13.9	4.1	3.9	2.8	3.5	30	3.4
58 2 2903	AR	.033	126	694	318	4.1	4.0	3.0	.00	692	510	13.9	4.1	3.9	2.8	3.5	30	3.4
58 2 3503	AR	.033	125	690	318	4.1	3.9	2.9	.00	693	510	21.0	4.1	3.9	2.7	5.4	22	4.3
58 2 4103	AR	.033	126	689	317	4.1	3.9	2.9	.00	694	510	21.1	4.1	3.9	2.7	5.4	20	4.7
58 2 4700	AR	.033	127	689	316	4.1	3.9	3.0	.00	690	510	27.6	4.1	3.9	2.6	7.0	10	8.3
58 2 5301	AR	.033	126	688	318	4.1	4.0	3.0	.00	690	510	27.6	4.1	4.0	2.6	7.0	9	7.5
58 2 5900	AR	.033	128	692	316	4.1	4.0	3.0	.00	695	510	34.7	4.1	3.9	2.5	8.8	5	12.5
58 2 6499	AR	.033	128	693	316	4.1	4.0	3.0	.00	689	510	34.7	4.1	3.9	2.5	8.8	4	13.6
58 2 7099	AR	.033	127	691	318	4.1	3.9	3.0	.00	691	510	41.4	4.2	4.0	2.5	10.4	3	12.2
58 2 7698	AR	.033	127	689	318	4.1	3.9	3.0	.00	688	510	41.4	4.1	3.9	2.4	10.5	3	11.9
58 2 8298	AR	.033	127	688	317	4.1	3.9	3.0	.00	691	510	48.4	4.2	4.0	2.4	12.1	4	11.1
58 2 8897	AR	.033	128	678	316	4.1	3.9	3.0	.00	690	510	48.4	4.1	3.9	2.4	12.3	4	10.3
58 2 9496	AR	.033	128	692	316	4.1	3.9	3.0	.00	690	510	55.2	4.1	3.9	2.3	14.1	9	8.5
58 210094	AR	.033	128	685	316	4.1	3.9	3.0	.00	691	510	55.3	4.1	4.0	2.3	14.0	8	8.9
59 2 499	AR	.033	126	687	321	4.1	3.9	3.0	.00	693	510	7.2	4.1	3.9	2.9	1.8	29	3.4
59 2 1099	AR	.033	126	698	320	4.1	4.0	2.9	.00	687	510	6.8	4.1	4.0	2.9	1.7	30	3.5
59 2 1700	AR	.033	125	701	320	4.1	3.9	2.9	.00	688	510	6.8	4.1	4.0	2.9	1.7	32	3.3
59 2 2302	AR	.033	127	693	318	4.1	3.9	2.9	.00	691	510	5.1	4.1	3.9	2.9	1.3	9	8.0
59 2 2901	AR	.033	125	685	320	4.1	3.9	2.9	.00	704	510	5.1	4.1	3.9	2.9	1.3	8	7.4
59 2 3503	AR	.033	125	694	320	4.1	3.9	2.9	.00	695	510	8.9	4.1	4.0	2.9	2.2	50	2.2
59 2 4103	AR	.033	126	684	320	4.1	3.9	2.9	.00	686	510	8.9	4.1	3.9	2.9	2.3	49	2.2
59 2 4702	AR	.033	127	687	319	4.1	3.9	2.9	.00	691	510	10.4	4.1	3.9	2.9	2.6	54	2.1
59 2 5302	AR	.033	126	689	320	4.1	3.9	2.9	.00	691	510	10.3	4.1	4.0	2.9	2.6	55	2.0
59 2 5902	AR	.033	126	693	319	4.1	3.9	2.9	.00	690	510	12.3	4.1	4.0	2.8	3.1	37	3.0
59 2 6502	AR	.033	126	692	319	4.1	3.9	2.9	.00	692	510	12.3	4.1	4.0	2.8	3.1	38	2.9
59 2 7101	AR	.033	126	693	320	4.1	3.9	2.9	.00	690	510	12.3	4.1	3.9	2.8	3.1	38	2.8
59 2 7701	AR	.033	125	685	321	4.1	3.9	2.9	.00	694	510	13.7	4.1	3.9	2.8	3.5	32	3.1
59 2 8300	AR	.033	126	687	319	4.1	3.9	3.0	.00	689	510	13.7	4.1	3.9	2.8	3.5	32	3.3
59 2 8900	AR	.033	127	693	319	4.1	3.9	2.9	.00	687	510	15.5	4.1	3.9	2.7	4.0	28	3.8
59 2 9499	AR	.033	127	685	319	4.1	3.9	3.0	.00	689	510	15.5	4.1	3.9	2.8	3.9	28	3.6
59 210098	AR	.033	126	689	319	4.1	3.9	2.9	.00	690	510	17.3	4.1	3.9	2.7	4.4	25	4.1
59 210698	AR	.033	126	690	321	4.1	3.9	3.0	.00	689	510	17.3	4.1	3.9	2.7	4.4	25	3.9
60 2 1055	AR	.058	125	560	316	4.1	4.0	3.3	.00	562	510	7.6	4.1	4.0	3.2	1.9	81	1.4
60 2 1654	AR	.058	126	555	315	4.1	4.0	3.4	.00	560	510	7.2	4.1	4.0	3.2	1.8	83	1.4
60 2 2254	AR	.058	125	557	315	4.1	4.0	3.4	.00	556	510	13.9	4.1	4.0	3.1	3.5	38	2.8
60 2 2853	AR	.058	125	552	314	4.1	4.0	3.3	.00	557	510	13.9	4.1	4.0	3.1	3.5	39	2.8
60 2 3452	AR	.058	126	556	313	4.1	4.0	3.3	.00	553	510	27.7	4.1	4.0	2.8	7.0	23	4.6
60 4 1131	AR	.058	126	558	317	4.1	4.0	3.4	.00	551	510	27.6	4.1	4.0	2.8	7.0	16	5.9
60 4 1732	AR	.058	126	555	311	4.1	4.0	3.4	.00	556	510	12.2	4.1	4.0	3.1	3.0	33	3.3
60 4 2331	AR	.058	126	559	315	4.1	4.0	3.3	.00	554	510	12.2	4.1	4.0	3.1	3.0	31	3.3

ANL Neg. No. 900-2574

TEST NO.	GAS	NID	Q*	MF	TI	PI	PS	PE	Z	MF*	TG*	PG*	PI*	PS*	PE*	PG*/PS*	DT*	H*
60 4 2930	AR	.058	126	555	312	4.1	4.0	3.3	.00	553	510	10.6	4.1	4.0	3.1	2.6	44	2.6
60 4 3531	AR	.058	126	557	313	4.1	4.0	3.3	.00	556	510	10.6	4.1	4.0	3.1	2.7	44	2.4
60 4 4131	AR	.058	126	553	314	4.1	4.0	3.3	.00	555	510	9.0	4.1	4.0	3.1	2.3	65	1.8
60 4 4730	AR	.058	127	552	312	4.1	4.0	3.3	.00	551	510	8.9	4.1	4.0	3.1	2.2	62	1.9
60 4 5331	AR	.058	127	556	312	4.1	4.0	3.3	.00	556	510	4.9	4.1	4.0	3.3	1.2	8	7.8
60 4 5930	AR	.058	127	553	313	4.1	4.0	3.3	.00	554	510	4.9	4.1	4.0	3.3	1.2	9	8.0
60 4 6530	AR	.058	128	555	312	4.1	4.0	3.3	.00	553	510	20.6	4.1	4.0	2.9	5.1	18	5.2
60 4 7130	AR	.058	127	549	313	4.1	4.0	3.3	.00	553	510	20.6	4.1	4.0	2.9	5.1	18	5.4
61 2 469	AR	.058	128	532	321	4.1	4.0	3.4	.00	524	510	7.2	4.1	4.0	3.2	1.8	86	1.4
61 2 1069	AR	.058	129	532	315	4.1	4.0	3.3	.00	531	510	7.2	4.1	4.0	3.2	1.8	82	1.4
61 2 1669	AR	.058	128	531	314	4.1	4.0	3.4	.00	530	510	7.2	4.1	4.0	3.2	1.8	82	1.4
61 2 2268	AR	.058	128	534	312	4.1	4.0	3.3	.00	535	510	34.9	4.1	4.0	2.7	8.7	22	4.5
61 2 2868	AR	.058	128	533	312	4.1	4.0	3.3	.00	532	510	34.9	4.1	3.9	2.6	8.8	23	4.7
61 2 3468	AR	.058	128	533	313	4.1	4.0	3.3	.00	534	510	41.6	4.1	4.0	2.5	10.4	24	4.1
61 4 530	AR	.058	129	534	318	4.1	4.0	3.3	.00	533	510	41.6	4.1	4.0	2.5	10.4	24	4.2
61 6 386	AR	.058	128	530	316	4.1	4.0	3.3	.00	536	510	48.5	4.1	4.0	2.4	12.1	27	3.7
61 8 468	AR	.058	128	532	315	4.1	4.0	3.4	.00	531	510	48.5	4.1	4.0	2.3	12.1	28	3.8
6110 488	AR	.058	127	537	318	4.1	4.0	3.4	.00	533	510	55.1	4.1	4.0	2.2	13.8	29	3.8
6112 474	AR	.058	127	533	317	4.1	4.0	3.4	.00	532	510	55.2	4.1	4.0	2.2	13.8	28	3.9
62 2 496	AR	.058	127	415	312	4.1	4.0	3.7	.00	417	510	7.4	4.1	4.1	3.6	1.8	32	2.9
62 2 1096	AR	.058	126	421	308	4.1	4.0	3.7	.00	414	510	7.4	4.1	4.0	3.6	1.8	32	3.3
62 2 1697	AR	.058	127	417	304	4.1	4.0	3.7	.00	417	510	7.4	4.1	4.0	3.5	1.8	33	3.2
62 2 2297	AR	.058	126	419	307	4.1	4.0	3.7	.00	417	510	14.2	4.1	4.0	3.4	3.5	16	5.5
62 2 2897	AR	.058	127	415	307	4.1	4.0	3.7	.00	416	510	14.3	4.1	4.0	3.4	3.5	17	5.3
62 2 3497	AR	.058	126	413	307	4.1	4.0	3.7	.00	417	510	20.7	4.1	4.1	3.3	5.1	14	5.6
62 2 4098	AR	.058	127	418	307	4.1	4.0	3.7	.00	413	510	20.7	4.1	4.0	3.3	5.1	15	6.2
62 2 4699	AR	.058	125	416	308	4.1	4.0	3.7	.00	419	510	27.4	4.1	4.0	3.2	6.8	17	5.0
62 2 5299	AR	.058	127	418	308	4.1	4.0	3.7	.00	419	510	27.4	4.1	4.1	3.2	6.8	17	5.3
62 2 5900	AR	.058	127	419	307	4.1	4.0	3.7	.00	415	510	34.7	4.1	4.0	3.1	8.6	16	5.8
62 2 6501	AR	.058	126	419	317	4.1	4.0	3.6	.00	422	510	34.7	4.3	4.2	3.3	8.2	15	5.5
62 2 7102	AR	.058	126	415	320	4.1	4.0	3.7	.00	420	510	41.9	4.1	4.1	3.0	10.3	17	4.8
62 2 7702	AR	.058	127	419	318	4.1	4.0	3.7	.00	434	510	42.2	4.2	4.2	3.1	10.1	16	4.9
62 4 467	AR	.058	128	417	313	4.1	4.0	3.7	.00	421	510	48.6	4.1	4.1	2.9	11.9	16	5.3
62 4 1067	AR	.058	127	416	322	4.1	4.0	3.7	.00	422	510	48.6	4.1	4.1	2.9	11.9	17	5.2
62 4 1667	AR	.058	128	416	320	4.1	4.0	3.7	.00	411	510	55.3	4.1	4.1	2.8	13.6	18	5.6
62 6 446	AR	.058	127	421	323	4.1	4.0	3.7	.00	435	510	55.4	4.1	4.1	2.8	13.6	17	4.8
63 2 522	AR	.058	128	415	315	4.1	4.0	3.7	.00	414	510	6.9	4.1	4.0	3.6	1.7	44	2.5
63 2 1122	AR	.058	128	412	313	4.1	4.0	3.7	.00	417	510	6.9	4.1	4.0	3.6	1.7	48	2.3
63 2 1721	AR	.058	126	418	312	4.1	4.0	3.7	.00	419	510	6.9	4.1	4.0	3.6	1.7	50	2.2
63 2 2322	AR	.058	127	418	310	4.1	4.0	3.7	.00	416	510	5.3	4.1	4.0	3.6	1.3	114	1.1
63 2 2921	AR	.058	126	417	311	4.1	4.0	3.6	.00	422	510	5.3	4.1	4.0	3.6	1.3	114	1.0
63 2 3521	AR	.058	126	418	312	4.1	4.0	3.7	.00	421	510	4.8	4.1	4.0	3.6	1.2	86	1.3

ANL Neg. No. 900-2569

TEST NO.	GAS	NID.	Q*	MF	TI	PI	PS	PE	Z	MF*	TG*	PG*	PI*	PS*	PE*	PG*/PS*	DT*	H*
63 2 4121	AR	.058	127	416	311	4.1	4.0	3.7	.00	420	510	4.8	4.1	4.0	3.6	1.2	88	1.3
63 2 4721	AR	.058	127	415	310	4.1	4.0	3.7	.00	420	510	5.8	4.1	4.0	3.6	1.4	100	1.2
63 2 5321	AR	.058	127	420	311	4.1	4.0	3.7	.00	417	510	5.8	4.1	4.0	3.6	1.4	103	1.2
63 2 5921	AR	.058	128	416	308	4.1	4.0	3.7	.00	416	510	8.7	4.1	4.0	3.5	2.2	27	3.9
63 2 6521	AR	.058	127	420	311	4.1	4.0	3.7	.00	416	510	8.7	4.1	4.0	3.5	2.2	25	4.0
63 2 7121	AR	.058	127	417	308	4.1	4.0	3.7	.00	420	510	10.3	4.1	4.0	3.5	2.6	21	4.4
63 2 7721	AR	.058	126	416	310	4.1	4.0	3.7	.00	418	510	10.3	4.1	4.0	3.5	2.5	21	4.2
63 2 8321	AR	.058	127	415	310	4.1	4.0	3.7	.00	417	510	12.4	4.1	4.0	3.5	3.1	18	4.7
63 2 8921	AR	.058	127	420	308	4.1	4.0	3.7	.00	416	510	12.4	4.1	4.0	3.5	3.1	18	5.3
67 2 518	AR	.084	127	695	322	4.1	3.9	2.9	.00	697	510	7.2	4.1	3.9	2.4	1.8	68	1.7
67 2 1117	AR	.084	127	693	320	4.1	3.9	2.9	.00	702	510	7.3	4.1	3.9	2.5	1.9	61	1.8
67 2 1715	AR	.084	128	692	317	4.1	3.9	2.9	.00	700	510	7.3	4.1	3.9	2.6	1.9	49	2.3
67 2 2313	AR	.084	126	695	321	4.1	3.9	2.9	.00	686	510	13.7	4.2	4.0	2.1	3.4	26	3.7
67 4 524	AR	.084	127	693	326	4.1	3.9	2.9	.00	701	510	13.7	4.1	3.9	2.0	3.5	33	3.2
67 6 450	AR	.084	128	690	324	4.1	3.9	2.9	.00	685	510	20.8	4.1	3.9	1.4	5.4	29	3.5
67 8 477	AR	.084	128	694	323	4.1	3.9	2.9	.00	699	510	20.8	4.1	3.9	1.4	5.3	26	3.7
6710 477	AR	.084	127	693	322	4.1	3.9	2.9	-.32	700	510	7.1	4.1	4.0	2.5	1.8	54	2.1
6710 1075	AR	.084	127	706	323	4.1	3.9	2.9	-.32	707	510	7.2	4.1	3.9	2.5	1.8	45	2.5
6710 1674	AR	.084	128	701	319	4.1	3.9	2.9	-.32	709	510	10.4	4.1	3.9	2.3	2.7	57	2.0
6710 2273	AR	.084	127	696	321	4.1	3.9	2.9	-.32	702	510	10.5	4.1	3.9	2.3	2.7	56	2.0
6710 2871	AR	.084	128	694	318	4.1	3.9	2.9	-.32	699	510	13.9	4.1	3.9	2.3	3.6	52	2.2
6712 464	AR	.084	128	695	320	4.1	3.9	2.9	-.32	706	510	14.0	4.1	3.9	2.1	3.5	46	2.4
6714 470	AR	.084	126	692	324	4.1	3.9	2.9	-.32	708	510	20.4	4.1	3.9	1.5	5.2	39	2.6
6716 483	AR	.084	127	693	324	4.1	3.9	2.9	-.32	692	510	20.4	4.1	3.9	1.5	5.2	40	2.6
6718 464	AR	.084	128	691	320	4.1	3.9	2.9	-.32	690	510	17.0	4.1	3.9	1.8	4.3	31	3.5
6720 500	AR	.084	128	691	322	4.1	3.9	2.9	-.32	700	510	17.1	4.0	3.8	1.7	4.5	27	3.7
68 2 460	AR	.084	128	694	321	4.1	3.9	2.9	.32	695	510	7.0	4.1	3.9	2.4	1.8	44	2.6
68 2 1056	AR	.084	127	701	320	4.1	3.9	2.9	.32	705	510	7.1	4.1	3.9	2.5	1.8	54	2.1
68 4 460	AR	.084	127	692	319	4.1	3.9	2.9	.32	692	510	10.7	4.1	3.9	2.3	2.7	42	2.8
68 6 451	AR	.084	129	690	320	4.1	3.9	2.9	.32	698	510	10.4	4.1	3.9	2.4	2.7	51	2.3
68 6 1048	AR	.084	129	700	318	4.1	3.9	2.9	.32	705	510	14.1	4.0	3.9	2.2	3.6	41	2.7
68 6 1647	AR	.084	129	694	318	4.1	3.9	2.9	.32	697	510	14.1	4.1	3.9	2.2	3.6	19	4.8
68 6 2245	AR	.084	126	693	321	4.1	3.9	2.9	.32	699	510	17.4	4.1	3.9	2.1	4.5	25	3.8
68 8 517	AR	.084	127	698	324	4.1	3.9	2.9	.32	689	510	17.4	4.1	3.9	2.0	4.4	21	4.7
6810 498	AR	.084	127	694	323	4.1	3.9	2.9	.63	698	510	7.0	4.1	3.9	2.4	1.8	38	2.7
6810 1096	AR	.084	126	700	322	4.1	3.9	2.9	.63	703	510	7.1	4.1	4.0	2.5	1.8	51	2.2
6810 1695	AR	.084	126	702	321	4.1	3.9	2.9	.63	693	510	10.4	4.1	3.9	2.2	2.7	24	4.4
6810 2293	AR	.084	127	697	321	4.1	3.9	2.9	.63	697	510	10.6	4.1	3.9	2.4	2.7	45	2.4
6810 2891	AR	.084	127	694	318	4.1	3.9	2.9	.63	697	510	13.9	4.0	3.9	2.1	3.6	22	4.5
6810 3490	AR	.084	127	694	318	4.1	3.9	2.9	.63	697	510	13.9	4.0	3.9	2.2	3.6	29	3.6
6810 4090	AR	.084	127	689	318	4.1	3.9	2.9	.63	697	510	17.7	4.1	3.9	2.2	4.5	19	5.3
6812 517	AR	.084	128	693	320	4.1	3.9	2.9	.63	688	510	17.4	4.1	3.9	1.7	4.4	14	7.3

ANL Neg. No. 900-2573

ACKNOWLEDGMENTS

We wish to acknowledge our indebtedness to R. P. Carter, who, as the principal designer on the job, gave valuable assistance in the design and fabrication of the test section and the various other components.

REFERENCES

1. B. M. Hoglund, R. P. Anderson, and L. Bova, *Experimental Study of a Gas Jet Penetrating a Liquid Coolant and Impinging on a Heated Surface*, ANL-7734 (Mar 1971).

2. H. K. Fauske, T. C. Chawla, A. W. Cronenberg, and J. F. Marchaterre, *Coolant Voiding and Pressure Generation Due to Boiling, Fission Gas Release, and Molten Fuel-Coolant Interaction*, Trans. Am. Nucl. Soc. *13*(2), 656-657 (Nov 1970).

3. T. C. Chawla and B. M. Hoglund, *Pressure Distribution for Axisymmetric Two-Dimensional Flow in a Plenum During Coolant Expulsion*, Nucl. Sci. Eng. *43*(1), 87-90 (Jan 1971).

4. T. C. Chawla and B. M. Hoglund, *A Study of Coolant Transients During a Rapid Fission Gas Release in a Fast Reactor Subassembly*, Nucl. Sci. Eng. *44*(3), 320-344 (Mar 1971).

5. R. E. Wilson, J. B. van Erp, and H. K. Fauske, *Heat Transfer to a Flowing Sodium-Gas Mixture*, Trans. Am. Nucl. Soc. *14*(1), 244 (1971).

6. J. B. van Erp, C. J. Roop, and P. L. Zaleski, *Simulation of Slow Fission Gas Release in an LMFBR Fuel Subassembly*, Trans. Am. Nucl. Soc. *14*(1), 277 (1971).

7. T. C. Chawla, J. B. van Erp, C. Fiala, and H. K. Fauske, *Coolant Expulsion and Reentry Following Rapid Fission-Gas Release in LMFBR Subassemblies*, Trans. Am. Nucl. Soc. *14*(2), 730 (1971).

8. R. E. Wilson, J. B. van Erp, T. C. Chawla, and E. L. Kimont, *Experimental Evaluation of Fission-Gas Jet-Impingement in LMFBR Subassemblies*, Trans. Am. Nucl. Soc. *15*(1), 348 (1972).

9. T. C. Chawla, R. E. Wilson, and J. B. van Erp, *Heat Transfer Coefficient Correlation for Liquid-Metal Spray Cooling Relative to Fission-Gas Jet-Impingement in LMFBR Subassemblies*, Trans. Am. Nucl. Soc. *15*(1), 349 (1972).

10. E. L. Kimont, R. E. Wilson, and J. B. van Erp, *Nondestructive Testing and Post-Mortem Examination of Heaters for LMFBR Fuel Pin Simulation*, Trans. Am. Nucl. Soc. *15*(1), 367 (1972).

11. T. C. Chawla, *Analysis of Inertial Contribution of the Fluid in a Plenum to a Rapid Coolant-Expulsion Process in an LMFBR Single-Subassembly Accident*, Nucl. Sci. Eng. *48*(4), 397-402 (Aug 1972).

12. T. C. Chawla, *On Equations of Motion for a Liquid-submerged Sonic Gas Jet and the Effect of Density Ratio on the Instability of the Gas-Liquid Interface Relative to Fission-gas Jet Impingement in LMFBR Subassemblies* (to be published as ANL report).

13. T. C. Chawla, *Liquid Entrainment Rate and Droplet Size Relative to Fuel Failure Propagation Due to Fission-Gas Jet-Impingement in LMFBR Subassemblies*, ASME paper No. 72, WA/NE-7 (Nov 1972).

14. J. B. van Erp, T. C. Chawla, and R. E. Wilson, *Potential Fuel Failure Propagation Due to Fission-Gas Release in LMFBR Subassemblies*, ASME paper No. 72, WA/NE-14 (Nov 1972).